UTILIZING A CYCLE SIMULATION TO EXAMINE THE USE OF THE EXHAUST GAS RECIRCULATION (EGR) SYSTEM FOR A SPARK-IGNITION ENGINE INCLUDING THE SECOND LAW OF THERMODYNAMICS

A Thesis

by

RAJESHKUMAR SHYANI

Submitted to the Office of Graduate Studies of
Texas A&M University
in partial fulfillment of the requirements for the degree of

MASTER OF SCIENCE

August 2008

Major Subject: Mechanical Engineering

UTILIZING A CYCLE SIMULATION TO EXAMINE THE USE OF THE EXHAUST GAS RECIRCULATION (EGR) SYSTEM FOR A SPARK-IGNITION ENGINE INCLUDING THE SECOND LAW OF THERMODYNAMICS

A Thesis

by

RAJESHKUMAR SHYANI

Submitted to the Office of Graduate Studies of
Texas A&M University
in partial fulfillment of the requirements for the degree of

MASTER OF SCIENCE

Approved by:

Chair of Committee,	Jerald A. Caton
Committee Members,	Jorge Alvarado
	Timothy Jacobs
Head of Department,	Dennis O' Neal

August 2008

Major Subject: Mechanical Engineering

ABSTRACT

Utilizing a Cycle Simulation to Examine the Use of the Exhaust Gas Recirculation (EGR) System for a Spark-ignition Engine Including the Second Law of Thermodynamics.

(August 2008)

Rajeshkumar Shyani, B.E., Mechanical Engineering, Sardar Patel University, India

Chair of Advisory Committee: Dr. Jerald A. Caton

The exhaust gas recirculation (EGR) system has been widely used to reduce nitrogen oxide (NOx) emission, improve fuel economy and suppress knock by using the characteristics of charge dilution. However, previous studies have shown that as the EGR rate at a given engine operating condition increases, the combustion instability increases. The combustion instability increases cyclic variations resulting in the deterioration of engine performance and increasing hydrocarbon emissions. Therefore, the optimum EGR rate should be carefully determined in order to obtain the better engine performance and emissions. A thermodynamic cycle simulation of the four-stroke spark-ignition engine was used to determine the effects of EGR on engine performance, emission characteristics and second law parameters, considering combustion instability issues as EGR level increases. A parameter, called 'Fuel Fraction Burned,' was introduced as a function of the EGR percentage and used in the simulation to incorporate the combustion instability effects. A comprehensive parametric investigation was conducted to examine the effects of variations in EGR, load and speed for a 5.7 liter spark-ignition automotive engine. Variations in the thermal efficiencies, brake specific NOx emissions, average combustion temperature, mean exhaust temperature, maximum temperature and relative heat transfer as functions of exhaust gas recycle were determined for both cooled and adiabatic EGR configurations. Also effects of variations in the load and speed on thermal efficiencies, relative heat transfers and destruction of availability due to combustion were determined for 0% EGR and 20% EGR cases with both cooled and adiabatic configurations.

For both EGR configurations, thermal efficiencies first increase, reach a maximum at about 16% EGR and then decrease as the EGR level increases. Thermal efficiencies are slightly higher for cooled EGR configuration than that for adiabatic configuration. Concentration of nitric oxide emissions decreases from about 2950 ppm to 200 ppm as EGR level increases from 0% to 20% for cooled EGR configuration. The cooled EGR configuration results in lower nitric oxide emissions relative to the adiabatic EGR configuration. Also second law parameters show the expected trends as functions of EGR. Brake thermal efficiency is higher for the 20% EGR case than that for the no EGR case over the range of load (0 to WOT) and speed (600 rpm to 6000 rpm).

Predictions made from the simulation were compared with some of the available experimental results. Predicted thermal efficiencies showed a similar trend when compared to the available experimental data. Also, percentage of unused fuel availability increases as the EGR level increases, and it can be seen as one of the effects of deteriorating combustion quality as the EGR level increases.

DEDICATION

I would like to dedicate this thesis to my parents who have been a major influence in my life. They have supported me wholeheartedly in all my endeavors. I would also like to dedicate the thesis to my late grandparents who provided me continuous inspiration and whose encouragement has kept me going throughout my academic life.

ACKNOWLEDGMENTS

I would like to express the deepest appreciation to my committee chair, Dr. Jerald Caton, who has the attitude and the substance of a genius: he continually and convincingly conveyed a spirit of enthusiasm in regard to research. Without his guidance and persistent help this thesis would not have been possible.

I would also like to thank my committee members, Dr. Timothy Jacobs and Dr. Jorge Alvarado, whose cooperation and support allowed me to finish this work within the various constraints of time and resources.

Finally, I would like to thank Texas A&M University and express my gratitude to everyone who helped and supported me in my current endeavor.

NOMENCLATURE

a	specific availability
A	system total availability
a_f	specific flow availability
h	enthalpy
h_{in}	enthalpy into the system
h_{out}	enthalpy out of the system
m	total cylinder charge mass
$\dot{m}_a$	mass flow rate into adiabatic zone
$\dot{m}_{bl}$	mass flow rate into boundary layer
$\dot{m}_{in}$	mass flow rate into the system
$\dot{m}_{out}$	specific internal energy of adiabatic zone
$\dot{m}_u$	mass flow rate into unburned zone
$p(\theta)$ or p	instantaneous cylinder pressure
$\dot{Q}$	heat transfer rate to the cylinder gases
r	compression ratio
t	time
$T(\theta)$ or T	instantaneous cylinder gas temperature
T_a	instantaneous adiabatic zone gas temperature
T_{avg}	instantaneous average cylinder gas temperature
T_b	instantaneous burned zone gas temperature
T_u	instantaneous unburned zone gas temperature
T_{exh}	average exhaust temperature
T_{wall}	wall temperature
u	specific internal energy
u_a	specific internal energy of adiabatic zone
u_b	specific internal energy of burned zone

u_{bl}	specific internal energy of boundary layer zone
v	specific volume
V	cylinder volume
$\dot{W}_b$	brake power

Greek and other symbols:

θ	instantaneous crank angle
θ_o	crank angle of start of combustion
θ_{end}	crank angle of end of combustion
ϕ	fuel-air equivalence ratio
η	thermal efficiency
η_{max}	maximum thermal efficiency

Abbreviations

AF or A/F	air to fuel mass ratio
bmep	brake mean effective pressure
bsfc	brake specific fuel consumption
CA	crank angle
CDS	combustion duration schedule
DOHC	dual over head camshafts
EGR	exhaust gas recirculation (eq. 4)
EVC	exhaust valve close
EVO	exhaust valve open
FFB	Fuel Fraction Burned (eq. 5)
FFBS	fuel fraction burned schedule
imep	indicated mean effective pressure
IVC	intake valve close
IVO	intake valve open
LHV	lower heating value of the fuel

MBT	the start of combustion timing which provides the Maximum Brake Torque
ppm	part per million (concentration)

TABLE OF CONTENTS

Page

Page

LIST OF FIGURES

Page

Page

Page

LIST OF TABLES

Page

1. INTRODUCTION

NOx is one of the primary pollutants emitted from combustion processes. NOx is a generic term for mono nitrogen oxides (NO and NO_2). Scientific studies of the late 1960s discovered that NOx was adding to smog (a significant form of air pollution) and ozone production. It combines with moisture in the atmosphere to produce HNO_3 (a component of acid rain), it increases the risk of respiratory diseases, and it causes pulmonary and respiratory problems.

In the 1970s manufacturers were designing their engines for lower HC and CO emissions. Unfortunately the resulting lean air-fuel mixtures and higher engine operating temperatures raised NOx in the exhaust. After realizing the harmful effects of NOx, the Environmental Protection Agency (EPA) added NOx to its list of regulated items. Environmental regulations are the driver forcing industry to implement NOx control techniques. Standards for the control of NOx have been established as part of the Clean Air Act starting in 1970. The Clean Air Amendments of 1990, and in particular, Title I (Ozone Attainment), Title IV (Acid Rain) and New Source Review requirements have resulted in various State Implementation Plans aimed at reducing NOx. In the year 2002, EPA forced the engine manufacturers to produce the engines that the exhaust from newly manufactured engines (typically heavy diesel engines) must produce half the oxides of nitrogen (NOx) of engines produced those days with no increase in particulate matter (PM). The accelerated requirement was the fruit of a settlement the EPA arranged with diesel engine manufacturers in late 1998 upon threat of protracted litigation.

1.1 Comparison of Diesel and Gasoline Engine on Emissions Basis

The chemical pathways of the formation of nitric oxides and their destruction in flames provide the basis for the development of design strategies for low emission combustion sources. The design strategy varies according to the fuel type (gasoline or

---

This thesis follows the format and style of *Journal of Automobile Engineering*.

diesel). Table 1 shows a comparison of the pollutant patterns of gasoline (Otto) engines and diesel engines for two operating modes [**1**]. In this table, the differences in emission patterns under idle conditions and under normal cruise conditions for the two types of engines are shown.

Under cruise conditions, a diesel cycle system produces significantly higher overall NOx emissions than a spark ignited or Otto cycle engine. At idle conditions, the NOx emissions from the compression ignition (diesel) engines are much lower than for the spark ignited engines. With respect to hydrocarbons and carbon monoxide, the emissions from the spark ignited engines are significantly higher, in some cases by an order of magnitude, than diesel engines, due to the excess air and compression conditions in a diesel engine. Carbonaceous particulate formation for diesel engines is significantly greater than for spark ignited engines, due to oily nature of diesel fuels (heterogeneous combustion process) and higher molecular weight.

Table 1 Typical IC engine pollutant concentrations [**1**]

Contaminant	Engine Type	Cruise Mode	Idle Mode
NOx, ppm	Diesel	1400	50
	Otto	500	100
HC, ppm	Diesel	100	200
	Otto	6000	4000
CO, ppm	Diesel	500	150
	Otto	60000	10000
Soot	Diesel	High	High
	Otto	Low	Low

1.2 NOx Reduction Techniques

The engine operating parameters like air-to-fuel ratio, spark timing, compression ratio, engine speed, engine power, engine temperature, engine cleanliness etc. affect the amount of NOx emissions from the combustion process. Also engine design parameters like surface to volume ratio, exhaust back pressure, valve overlap, and fuel injection have an impact on the NOx emissions. Apart from adjusting these parameters to reduce the NOx emissions, the techniques like exhaust gas recirculation (EGR) and catalytic converter are used to reduce the amount of NOx emissions.

From the knowledge of parameters affecting the NOx emissions, some of the methods to reduce the NOx emissions can be suggested [**2**]:

a) Derating

NOx formation mainly depends on temperature conditions in the cylinder. The pressure and thereby temperature in the cylinder can be reduced by operating the engine using a smaller supply of fuel (diesel engine) or by using a lean air-fuel mixture

b) Retarded Ignition Timing

For spark ignited IC Engines, the influence of retarding or advancing the spark timing may be significant. If the spark timing is advanced, the overall temperatures during the cycle tend to go up and NOx emissions will therefore increase. Retarding the spark timing tends to lower oxides of nitrogen but may not reduce hydrocarbon emissions marginally.

c) Air-to-fuel Ratio Adjustment

In a stoichiometric air-fuel ratio, the oxygen in the air-fuel mixture should completely oxidize the fuel. However, the oxygen content in the stoichiometric state has been determined to be 1 percent by volume of oxygen in the exhaust gas. Under lean-burning conditions, the air-fuel ratio is higher than that in the stoichiometric state. Therefore, an engine operating in the lean burning conditions contains more than 1

percent by volume of oxygen in the exhaust gases; consequently NOx emissions will be higher, but HC and CO emissions are decreased. The air-fuel ratio is lower in the rich burning conditions than that in the stoichiometric state. The exhaust gases from a rich-burning engine contain less than 1 percent by volume of oxygen; NOx emissions will be lower, but HC and CO emissions are increased.

If the air-to-fuel ratio is decreased to achieve the rich-burning state, NOx formation will drop sharply, there being insufficient oxygen for combustion; and HC and CO emissions will increase accordingly.

d) Turbocharger with Intercooler (For Diesel Engines)

Turbocharger is the arrangement in which the exhaust gases from an engine are guided to a turbine that drives a compressor. The compressor compresses the intake air, which is cooled in an intercooler. Because of compression and the lower temperature of incoming air, a greater mass of air can be packed into the air manifold. Given the conditions of higher pressure and greater air mass, more fuel can be injected and burned, to produce more power for a given size of engine. The low temperature of the intake air leads to low peak temperature during combustion and thus to low NOx emissions. It has been reported that 10 to 30 percent NOx reduction has been achieved from diesel engines with the use of turbocharger with intercooler. Also, HC and CO emissions decrease because the turbocharger increases the air-fuel ratio to that of a lean burning mixture.

e) Reduced Manifold Air Temperature

As mentioned in the previous technique, the manifold air temperature can be reduced by using an intercooler upstream of the manifold. Greater air mass can be packed because of the high air density at low air temperature and thereby more fuel can be injected and burned to produce more power. When there is a low air temperature, peak combustion temperature also is low; therefore NOx emissions are low. But the

combustion reactions are slow at very low air temperature, so that HC and CO emissions increase.

f) Exhaust Gas Recirculation

Exhaust gas recirculation is the most widely used technique these days. This method involves recirculation of some of the exhaust gas to replace one portion of the intake air. External EGR is the recirculation of exhaust gas to the air manifold, whereas internal EGR is achieved by restricting a portion of the exhaust gas from exiting the cylinder. There are two configurations by which exhaust gas can be recirculated, cooled EGR and adiabatic EGR. Both configurations of the EGR will reduce the peak combustion temperature, thus lowering the NOx emissions. HC and CO emissions increase, because of a lack of available air for combustion and combustion instabilities.

g) Water Induction

Water is introduced into the engine either with the intake air or by water injection directly into the cylinder. The vaporization of this water helps to reduce the peak combustion temperature; thus, NOx emissions are low. But at low temperatures, hydrocarbons are burned slowly; therefore HC emissions increase. On the other hand, CO emissions are unaffected by water induction.

h) Combustion Chamber Redesign

Combustion chambers can be modified to have a cavity at the piston head or to have a bowl shaped cylinder head. Fuel is injected into the cavity (formed by a combustion chamber modification) as a rich mixture and ignited. NOx formation is delayed as the mixture burns in the absence of excess air. Then the burning mixture enters the main combustion chamber, and is mixed with additional air, to complete the combustion and lower the peak temperature. Therefore NOx emissions, as well as HC and CO emissions, are low.

i) Catalytic Converter

Three way converter (TWC) catalysts are used to reduce NOx, HC and CO emissions. Precious metal catalysts are used to oxidize HC and CO, and rhodium catalyst coverts NOx to N_2. By using a TWC catalyst, NOx, HC, and CO can be reduced simultaneously.

1.3 Concept of Combustion Quality

It is convenient to analyze the modes of operation in a cycle commencing with the gas exchange process (exhaust, charging) and following with the power process (compression, combustion, expansion). Each part of the cycle contributes to the overall indicated efficiency of the engine, and this contribution varies in degree according to how closely that portion of the cycle approaches an ideal process. For example, the faster a cycle completes its combustion near TDC, the greater its contribution to the overall efficiency.

Also, observation of cylinder pressure versus time measurements from a spark-ignition engine, for successive operating cycles, shows that substantial cycle-by-cycle variations exist. Since the pressure development is uniquely related to the combustion process, substantial variations in the combustion process on a cycle-by-cycle basis are occurring. In addition to these variations in each individual cylinder, there can be significant differences in the combustion process and pressure development between the cylinders in a multi-cylinder engine. Cyclic variations in the combustion process are caused by variations in mixture motion within the cylinder at the time of spark cycle-by-cycle, variations in the amounts of air and fuel fed to the cylinder each cycle, and variation in the mixing of fresh mixture and residual gases within the cylinder each cycle, specifically in the vicinity of the spark plug. Variations between cylinders are caused by differences in these same phenomena, cylinder-to-cylinder.

It is possible to classify cycles into groups in the order of their likely contributions to the overall efficiency, based on the time of completion of flame

propagation. Table 2 shows the classification of cycles based on the combustion completion.

Table 2 Classification of cycle based on flame propagation completion [**3**]

Flames Detected Between	**Type of Cycles**
-45^{o} and TDC	Early burn cycles
TDC and 45^{o}	Fast burn cycles
45^{o} and 90^{o}	Slow burn cycles
90^{o} and BDC	Late burn cycles
BDC and TDC	Delayed burn cycles
Flames not detected	Misfires and partial burn cycles

Misfire occurs when the mixture is too lean to ignite and there is no combustion whereas partial combustion occurs when the mixture is ignited but the rate of combustion is too slow to burn the charge completely within the power stroke.

1.3.1 Exhaust Gas Recirculation and Combustion Quality

It is apparent that it is difficult to eliminate HC and NOx emissions at the same time. Historically, efforts to reduce one have tended to increase the other. Nowadays almost all automotive engines use exhaust gas recirculation (EGR) to control the NOx emissions in combination with other techniques. The effects of EGR on the combustion stability (which can be directly related to cylinder pressure), and its subsequent effects on other performance parameters of engines are still a subject of concern and research. Therefore, the amount of exhaust gas recirculated is limited by engine performance since combustion quality and hence the engine performance deteriorates as the amount of exhaust gas recirculated increases beyond some level. The effects of exhaust gas

recirculation on combustion quality, efficiency, heat transfer and second law parameters along with NOx reduction were the major items to be considered in the present work.

In a spark-ignition engine, as the unburned mixture is leaned out with excess air or is diluted with increasing amounts of burned residual gas and exhaust gas recycle, the flame development period, flame propagation period, the duration of the rapid burning phase, and the cycle-by-cycle fluctuations in the combustion process all increase. Eventually a point is reached where engine operation becomes rough and unstable and hydrocarbon emission increase rapidly. The point at which these phenomena occur effectively defines the engine's stable operating limit. These phenomena result from the lengthening of all stages of the combustion process as the unburned mixture is diluted.

With increasing dilution, first a fraction of the cycles burns so slowly that combustion is only just completed prior to exhaust valve opening. Then as burning lengthens further, in some cycles there is insufficient time to complete combustion within the cylinder; also, flame extinguishment before the exhaust valve opens and before the flame has propagated across the chamber may start to occur in some cycles. Finally, misfiring cycles, where the mixture never ignites, may start to occur. The proportion of partial burning or non-burning cycles increases rapidly if the mixture is made even more lean or dilute, and the point is soon reached where the engine will not run at all.

Considering these effects of dilution, a parameter, called 'Fuel Fraction Burned (FFB)' as functions of EGR percentage, is proposed in the present work to incorporate the combustion instability effects. The proposed FFB schedule was such that the efficiency results from the simulation gave the similar trend as that from experimental results. Then this FFB schedule was used for the complete parametric study.

2. OBJECTIVES AND MOTIVATION

The overall objective of this research project is to determine engine performance and NOx emission concentrations considering the combustion instability effects at higher EGR levels and to analytically conduct a complete parametric study. The specific tasks to satisfy the primary objective are:

1) The first task of the present research project is to analyze the effects of EGR on the combustion stability. Previous model, used for a similar kind of study, does not include combustion instability issues at higher EGR levels. The extended model will have the ability to incorporate the effects of such combustion instabilities. The fraction of fuel burned as functions of EGR percentage is proposed and used to incorporate the effects of all kinds of combustion instabilities like slow burn, misfire and incomplete combustion.
2) The second task is to conduct a comprehensive parametric study of the effects of EGR levels (0%-40%) on engine performance. For this purpose, different FFB schedules are to be examined and the one which gives the best match with experimental results [**4**] will be used in this study. A complete parametric study includes efficiency, temperatures, NOx emission, relative heat transfer and second law parameters. The second law parameters include availability accountings viz. availability to indicated work, availability moved via heat transfer, availability destroyed due to combustion and availability out with exhaust. Some of these results from the simulation are expected to confirm the validity of the model.
3) The other important task of the present work is to include effects of variations in load and engine speed for 0% and 20% EGR (with corresponding FFB value) for both cooled and adiabatic configurations. This part of the work includes efficiency, relative heat transfer, temperatures and availability accountings as functions of load and engine speed.

One of the primary motivations of this project was the difference between the results from similar previous work and experimental results from the experiments for high levels of EGR. In the previous study, combustion instability issues were not included and it might be a reason for difference between the simulation results and the experimental results.

3. LITERATURE REVIEW

EPA works to develop and enforce regulations that implement environmental laws enacted by Congress. A major source of environmental pollution is automobiles and the EPA enforces the automobile industries to strictly meet the standards. To meet these requirements, industries conduct vast research through experiments and simulations. And therefore, even though the emissions standards become increasingly more difficult to meet, the automobile industries have always been able to continue to improve engine durability, reliability, performance, and fuel economy.

This section will provide a brief summary of the experimental and computational works concerning the use of EGR and its effects in SI engines. Some of the related work in CI (diesel) engine is also discussed in this section.

A large amount of the previous work concerning EGR as a technique to reduce the NOx emissions has been done primarily in the areas of EGR system design and its effects on the SI engine performance. Thermodynamic models have been developed in the past for SI engines, but fewer studies have indicated the use of these models for parametric studies of effects of EGR on combustion stabilities. Also, these limited parametric studies conducted in the past have been using several assumptions to reduce the complexity and hence they may not be accurate enough.

3.1 Previous Experimental Studies

A considerable amount of experimental work has been done to fully understand the working of EGR and its deteriorating effects on combustion stability at higher EGR levels.

The use of EGR in an engine operation was reported as early as 1940: Berger *et al.* [**5**] conducted an experimental study on the effects of exhaust gas contaminated inlet mixture which was motivated by applications of engines in underground mines. The experimental results showed increase in carbon monoxide and decrease of nitric oxides.

The engine experiments by Miller *et al.* [**6**] reported that EGR minimizes the problem of knock. The results from this study included a suppression of knock, a

reduction of full load performance and a decrease of exhaust gas temperatures with the addition of exhaust gas to the inlet charge. With respect to emissions, Kopa and Kimura [**7**] and Kopa *et al.* [**8**] appear to be among the first to describe experiments using EGR to investigate specifically the potential of reducing nitric oxide. This work was successful and subsequently many others provided results on the effects of EGR on engine performance and emissions. Although the use of EGR was effective for reducing nitric oxide, Kopa *et al.* [**8**] and Musser *et al.* [**9**] found this technique caused reduced engine power, increased the temperature of the inlet air, and increased engine wear.

The other authors noted that as the air-fuel mixture in a spark ignition engine is leaned out with increased amount of burned residual gas and exhaust gas recycle, the duration of overall combustion process and cycle-by-cycle fluctuations in the combustion process increase [**10, 11**]. Eventually a point is reached where engine operation becomes rough and unstable and hydrocarbon emissions increase rapidly. The actual effects of EGR on combustion show the occurrence of four kinds of combustion patterns (Normal Burn, Slow Burn, Partial Burn and Misfire), and those vary with the EGR level (see Appendix).

The impact on engine stability of increasing combustion variability, due to increased EGR at part-load was studied experimentally by Kuroda *et al.* [**10**]. The experimental study used the distribution of indicated mean effective pressure values for varying EGR levels to predict the engine stability. The results indicate the spread in imep is narrow without the use of EGR. Increasing EGR widens the distribution significantly and cycles with low imep and eventually zero imep, occur. Also results were obtained to determine how the coefficient of variation in imep (COV_{imep}[1]) and hydrocarbon emissions increase as EGR is increased. The results show increase in COV_{imep} from 4% to 10% as EGR increases from 0% to 18% (see Appendix). Some of the observations and conclusions of the study [**10**] regarding how the frequency of slow burn, partial burn and misfire occur with increasing EGR are as follows:

[1] $COV_{imep} = (100*\sigma_{imep})/ imep_{mean}$, where σ_{imep} is the standard deviation of imep. Engine stability problems usually occur when the COV_{imep} exceeds 10 per cent [**10**].

1) As the EGR level increases, slow burn cycles start to appear first at about 8% EGR. The engine stability deteriorates with the increase of slow burn cycles and at 5% slow burn (which occurs just before the onset of partial burn cycles) the engine reaches the acceptable stability limit. In the slow-burn cycles, combustion is complete but ends 80^{o} after TDC and the imep is low (between 85% and 46% of the mean value).
2) With further increase of EGR rate beyond the engine stability limit, partial burn cycles begin to appear at about 20% EGR. Once partial burn cycles appear, unburned charge is carried over to the next cycle as residual gas. This further increases fluctuation in the indicated mean effective pressure and the engine stability deteriorates rapidly. Imep of partial-burn cycles is less than 46% of the mean.
3) Misfire cycles appear at a much higher EGR rate, where partial burn cycles appear at the frequency of several percent and slow burn cycles appear at very high frequency. At this condition, because of the higher frequency of slow burn, deterioration in engine stability (variations in imep), fuel economy and HC emissions are very high. In misfiring cycles, imep is less than 0.

It was revealed from the experimental study [**10**] that the factor limiting the practical engine stability limit was neither misfire nor partial burn but the appearance of slow burn cycles at a frequency of about 5% (see Appendix). The reduced flame temperature due to higher EGR level tends to reduce the burning velocity. Due to decreased burning velocity combustion duration tends to be longer, which tends to be more susceptible to the factors causing combustion fluctuation.

Using COV_{imep} as the parameter for indication of combustion instabilities, Cha *et al.* [**11**] examined the effects of EGR on combustion stability, engine performance, NOx and the other exhaust emissions for a 1.5 liter DOHC gasoline engine. During the experimentation, EGR rate was slowly increased until it is limited to the acceptable COV_{imep} level at each test condition and spark timing was advanced over MBT point. The experiments showed that the formation of NOx emission rate could be reduced from

25.4% up to 89.6% with EGR. Some of the other conclusions of the study [**11**] are as follows:

1) BSFC decreases with the increase of EGR level except at very high levels of EGR.
2) For increasing EGR, not only flame propagation speed but also the peak gas temperature and pressure were decreased. Advancement in ignition timing is one of the ways to minimize the power loss and to achieve the stable combustion.
3) COV_{imep} increases as EGR rate increases, and it is decreased as spark timing is advanced. Therefore the spark timing corresponding to minimum COV_{imep} is advanced as EGR rate is increased.
4) Crank angle of maximum cylinder pressure (^{o}aTDC) can be retarded by application of EGR, because flame propagation speed decreases as EGR rate increases. Maximum pressure decreases in proportion to EGR rate, and increases as spark timing is more advanced. When EGR is applied, brake power decreases as the EGR rate increases, and it can be increased by advancing the spark timing. However, advancing the spark timing further from the MBT may cause brake power to decrease.

Experimental study by Gardiner *et al.* [**12**] found that by adding to the in-cylinder charge up to 11 percent hot recycled exhaust gases via reopening the exhaust valve, the peak in cylinder pressure increased, in contrast with experiments with the usual EGR. Similar observations have also been discussed by Lebel-Simon and Cottereau [**13**]. Also the composition of recycled exhaust gas changes due to incomplete combustion occurring in the previous cycles, the exhaust gases also contain unburned fuel that is carried over from the previous cycle to the current cycle, changing A/F and combustion behavior in the current cycle [**14, 15**].

An explanation of combustion phenomenon at the engine stable operating limit has been developed by Quader [**16**]. Engine experiments have defined the locations of the ignition limit line and the partial-burn limit line. At a given spark timing, progressive

leaning of the mixture (or progressive diluting the mixture with EGR) fed to the engine will lead to onset of misfire or to the onset of partial burning depending on the location of the lines and the spark timing selected. Also, it was concluded that for spark timings retarded relative to MBT, partial burning and not failure of flame initiation is the primary cause of unstable engine operation.

Deeter *et al.* [**17**] presented results from a comprehensive experimental project that showed how EGR could be used in conjunction with spark timing adjustments and EGR scheduling to minimize any full-load penalties. The experiments used between 15% and 22% EGR to obtain up to 80% reduction in NOx.

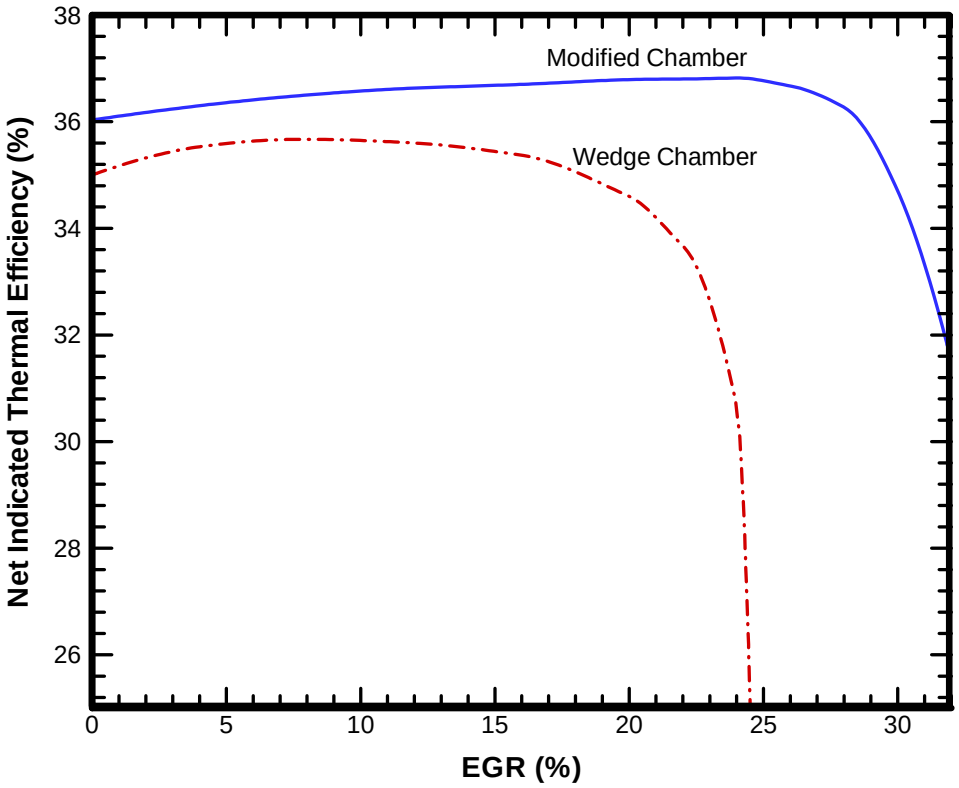

Fig. 1 Indicated thermal efficiency as functions of EGR for wedge chamber and modified chamber [**4**], (Redrawn)

Mattavi [**4**] reported on the efficiency trends for a 'Wedge Shaped' combustion chamber and a 'Modified Open' combustion chamber as functions of EGR percentage (Figure 1). The efficiency curves show a modest increase in the efficiency as the percentage of EGR increases at low levels of EGR but beyond certain EGR levels it shows a steep decrease in the efficiency for both types of combustion chamber designs. This implies that as EGR level increases it causes combustion instabilities due to the dilution effect which further leads to instable engine performance and reduction in efficiency.

In addition to the above SI engine work, research has been reported on the use of EGR with diesel engine. Jacobs *et al.* [**18**] examined the interactions resulting from the application and control of EGR on a heavy duty diesel engine system to understand their impact on NOx reduction, as well as reasons for potential negative side-effects. As EGR has an impact on "the intake charge side" of the engine, altering the amount of EGR will have deteriorating effects on combustion and hence on engine performance. There might be a fuel economy penalty associated with combustion deterioration. Also pumping work associated with the EGR flow might be as significant or more dominant under certain operating conditions. Also, the nitric oxide trends were examined to determine primary factors responsible for their reduction, such as thermal, dilution and dissociation effects.

Also, Ladommatos *et al.* [**19**] observed that in a diesel engine the displacement of inlet charge with CO_2 and H_2O (which are the main constituents of exhaust gas) can alter the combustion process in several ways, three of which are dilution effect, thermal effect and chemical effect of EGR. The reduction of O_2 concentration because of displacement brought by EGR within the engine cylinders that is available for combustion is referred to as the dilution effect. In the present work this effect may not be as significant as an equivalence ratio of 1 is assumed for the whole study. The thermal effect is referred to the higher specific heat capacities of both CO_2 and H_2O in comparison to that of O_2 being displaced. Both CO_2 and H_2O can, potentially, dissociate at the high temperatures prevailing during combustion and the products of dissociation participate in the

combustion process; this is referred to as the chemical effect of EGR. The experiments were conducted to quantify these three effects which can possibly affect the combustion process and emission. The results of the experiments show that reduction of inlet charge O_2 from 23.3 % to 16.3% by mass increases the ignition delay from about 8^o to almost 16^o CA. Although these results were obtained for a diesel engine, similar effects of increase in flame development and flame propagation period in spark ignition engine can be predicted as well. In the present work, the primary objective is to study the effects of EGR on engine performance including combustion instability issues for high levels of EGR.

3.2 Previous Computational Studies

The experimental studies concerning the use of EGR have been supported by numerous computational studies. After some initial experimental studies, Newhall [**20**] developed a detailed modeling project which helped describe the various effects of stoichiometry and compression ratio with the use of EGR.

The effects of EGR on engine performance, available energy and nitric oxide emissions for a spark ignition engine over a range of operating conditions were examined using a thermodynamic cycle simulation by Caton [**21**]. The simulation was conducted under certain assumptions to simplify the complex mechanisms of combustion. One such assumption was 100% combustion efficiency over the range of EGR from 0 to 40%. That means there is no unburned fuel at the end of combustion and there is no misfire. As the present work is the extension of this study with the combustion stability issues, some of the related results of the study are discussed below.

1) The nitric oxide emissions decrease rapidly with increasing EGR. The adiabatic EGR configuration results in higher nitric oxide emissions relative to the cooled EGR configuration since the gas temperatures are higher. However with the adiabatic EGR configuration, over 90% reduction in nitric oxide concentration is achieved with about 25% EGR.

2) For both EGR configurations, the indicated and brake thermal efficiencies increase with increasing percentage of EGR. In general, the brake thermal efficiency for the cooled EGR case is slightly higher than that for adiabatic EGR case. The brake thermal efficiency increases from about 25.7% to about 29% as the EGR rate increases from 0 to 40%. These results do not match with the experimental results [**4**]. This is due to the reason that combustion stability issues at higher EGR levels were not considered in the study [**21**].
3) Maximum cylinder gas temperatures, average combustion gas temperatures and average exhaust gas temperatures decrease as the percentage of EGR increases, and as expected, these three temperature measures are higher for the adiabatic configuration relative to the cooled configuration.
4) The brake thermal efficiency increases with increasing load due to the reduction in the throttle losses (*i.e.*, reduction of *pmep*). The maximum *bmep* results for the both EGR cases are lower than for no EGR, and are lowest for the adiabatic EGR case. The brake thermal efficiency for the EGR cases is higher than for no EGR case, and is similar for two EGR configurations.
5) For the 0% EGR case and the cooled 40% EGR case, the brake efficiency first increases, reaches a maximum (for engine speeds between about 1600 and 2000 rpm), and then decreases as engine speed increases. For the adiabatic EGR case the brake efficiency increases and reaches a maximum at about 2000 rpm (which is the WOT condition for adiabatic EGR case).

The present work reconsidered these results with the inclusion of combustion stability issues for higher EGR levels.

Aleiferis *et al.* [**22**] completed a computational study in conjunction with experimental study which included a sensitivity analysis of relative effects of local fuel concentration, residual gases, gas motion, spark energy, and heat losses to the electrodes on the level of cyclic variability in the early-flame development stage that corresponds to the 0-5 percent mass fraction burned duration. The calculated flame-radius evolutions

(from the flame images) were compared with the experimental data. This comparison suggested that a variation in air-fuel ratio of $\Delta(A/F) = 4$ (in terms of equivalence ratio ϕ, a variation $\Delta\phi = 0.15$) was large enough to account for 100 percent of the observed cyclic variability in flame-kernel radius. Also, a variation in the residual-gas fraction of about 20 percent around the mean was responsible for up to 30 percent of the measured cyclic variability.

3.3 Summary

As already stated earlier, fewer analytical studies have been conducted in the past which were primarily aimed at investigating the effects of EGR on NOx emissions. Experimental studies are both time consuming and extremely expensive. The analytical studies conducted in the past may be incomplete in the sense that studies were conducted with some assumptions to simplify the some of the complex phenomena.

There is a need for a more comprehensive study for the effects of EGR on NOx emissions considering its parallel effects on combustion stability. There is a need for a robust and a more detailed thermodynamic model, which can incorporate the cycle-by-cycle variation and combustion stability issues. The present research, however, aimed to conduct a complete parametric study considering the combustion instability issues taking previous work as reference [**10, 11**]. This parametric investigation will be more comprehensive than some of the previous studies. Effects of variations in EGR, load and engine speed will be conducted with both cooled and adiabatic EGR configurations. The engine performance parameters selected for the analysis are thermal efficiencies, mean exhaust temperature, maximum temperature, average combustion temperature, brake specific nitric oxide emissions, relative heat transfer and second law parameters.

4. SIMULATION DESCRIPTION

The development and use of computerized thermodynamic engine cycle simulations have been reported since the early 1960s. The original simulations were based on one-zone and two-zone formulations, and then these types of simulations were extended to include three or more zones. Patterson and van Wylen (1964) [**23**] reported one of the first thermodynamic simulations that included unburned and burned zones, progressive combustion, heat transfer, and flame propagation for uniform (homogeneous) charge engines. Their simulation did not, however, include flow rates, heat transfer from the unburned zone, and other features. Also, a significant amount of previous work on the use of the second law of thermodynamics with respect to engine operation has been reported over the last 50 years. Interestingly, the work by Patterson and van Wylen [**23**] included one of the first presentations of the results of an availability analysis. A summary of such investigations on availability analysis for reciprocating engines is available from Caton [**24**].

In the present study, a thermodynamic cycle simulation of a conventional spark-ignition engine operating on the four-stroke cycle was used. The simulation uses a multiple-zone combustion model, and also includes the second law of thermodynamics. This cycle simulation has been described in detail in the work by Caton [**25, 26**]. This simulation is largely based on thermodynamic formulations, and is a complete representation of the four-stroke cycle including the intake, compression, combustion, expansion and exhaust processes. The simulation uses detailed thermodynamic gas properties including equilibrium composition for the burned gases. The cylinder heat transfer is adopted from the correlation by Woschni [**27**], and the combustion process is based on a mass fraction burn relation from Wiebe [**28**]. Nitric oxide emissions are calculated using the extended Zeldovich kinetic [**29**] scheme.

Some of the inputs to the calculation are: engine geometry; compression ratio (r); engine speed (N); equivalence ratio (ϕ); percentage exhaust gas recycle fraction (%EGR); Fuel Fraction Burned (which is a function of % EGR); intake manifold

pressure (P_{in}), temperature (T_{in}) and start of combustion timing (θ_o), total combustion duration ($\Delta\theta_b$); and parameters which define the burning law. The cycle simulation then predicts the following: mass flow rate through the engine, cylinder pressure, unburned and burned mixture temperatures, heat transfer to the combustion chamber walls, work transfer to the piston, all as functions of crank angle during the cycle; and the indicated power, specific fuel consumption, thermal efficiency, mean effective pressure and mean exhaust temperature at the selected operating point. The cycle simulation also calculates second law parameters (availability values) for the complete cycle.

The next section summarizes the engine cycle simulation, and includes subsections on determining entropy and availability values. A description of the engine and operating conditions considered in this study are next.

4.1 Model Description

The features which are critical in interpreting the model predictions are briefly presented in this section. The key areas are: Basic assumptions; Combustion Model; Definition; and Method of Solution. Method of Solution includes a brief summary of Energy Equations, Heat Transfer, Friction Calculations, Nitric Oxide Computations, and Availability Parameters Calculations. Many of the features of the thermodynamic cycle simulation have been well documented elsewhere [**29-31**]. For simplicity, the combustion chamber was assumed to be a cylindrical shape. For this work, all cylinders of a multiple-cylinder engine are assumed to be identical, to possess the same thermodynamics, and to operate with identical conditions. This means, therefore, that overall results for a multiple-cylinder engine are obtained by multiplying the results from the single-cylinder analysis by the number of cylinders.

4.1.1 Basic Assumptions

The major assumptions and approximations used in the development include the following:

1) the cylinder contents constitute the thermodynamic system (see Figure 2).

2) the engine is in steady-state such that the thermodynamic state at the beginning of each cycle (two crank-shaft revolutions) is equivalent to the state at the end of the cycle.
3) the cylinder contents are spatially homogeneous and occupy one zone, for the compression, expansion and exhaust processes.
4) a two zones (each spatially homogeneous) model is used for intake process. One zone consists of the fresh charge and the other zone consists of the residual gases.
5) a three zones (each spatially homogeneous) model is used for the combustion processes. The three zones are: the unburned zone, the adiabatic core burned zone, and the boundary layer burned zone. The burned zone is comprised of the adiabatic core and the boundary layer zones.

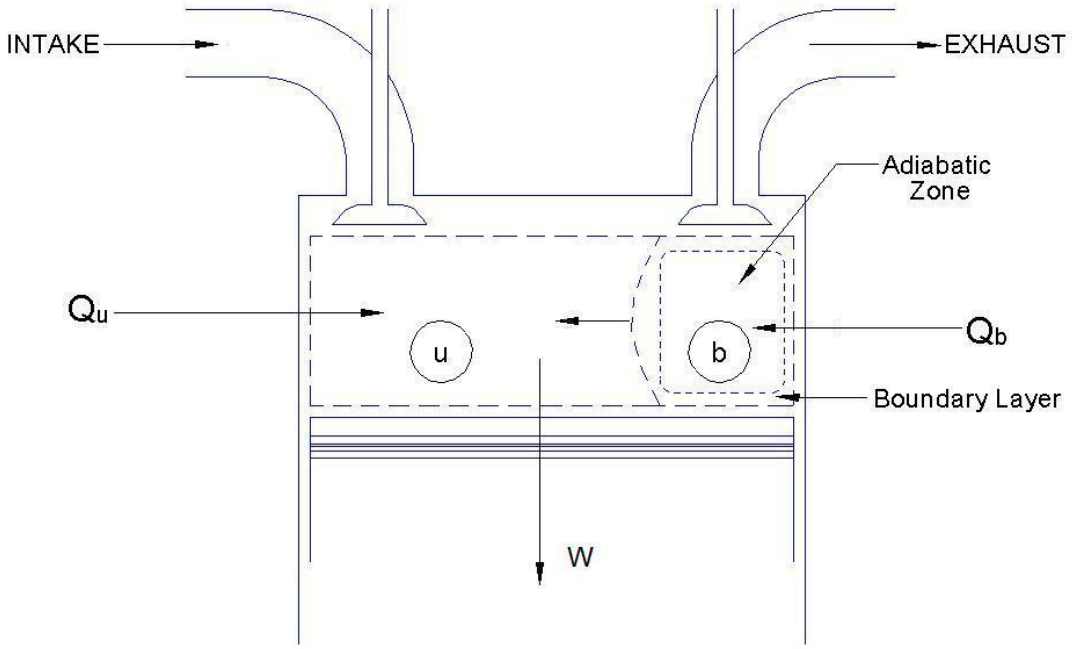

Fig. 2 A schematic of the cylinder depicting the three zones during combustion

6) the thermodynamic properties (including pressure and temperature) vary only with time (crank angle), and they are spatially uniform in each zone.
7) generally accepted algorithms [**29**] are used to calculate the instantaneous composition and the species obey the ideal gas equation of state.
8) the instantaneous thermodynamic properties are computed from established formulations [**29**] based on the appropriate compositions.
9) quasi-steady, one dimensional flow equations are used to determine the flow rates, and the intake and exhaust manifolds are infinite plenums containing gases at constant temperature and pressure.
10) the fuel is completely vaporized and mixed with the incoming air.
11) a parameter 'Fuel Fraction Burned' as functions of percentage of EGR is used to account for all kind of combustion instabilities.
12) the blow-by was zero.
13) exhaust gas recirculation (EGR) may be specified and the incoming charge will have a portion of combustion products from the previous cycle.
14) nitric oxide computations are included as described in a section of 'Method of Solution'.

The majority of the above assumptions and approximations have been validated and used in a number of previous simulations.

4.1.2 Combustion Model

The combustion model uses three zones to better capture the high temperatures during combustion which is critical to the nitric oxide computations. Figure 2 is a schematic of the engine cylinder which shows cylinder heat transfer, work, intake and exhaust flows, and two zones for the combustion process: an unburned (u) and a burned (b) zone. First, the formulation is developed for an unburned and burned zone. Then, the burned zone is expanded into an adiabatic zone and a boundary layer. At the start of the combustion process, the boundary layer has zero mass, and the adiabatic core is equal to

the burned mass. The boundary layer increases in mass by entraining mass from the adiabatic core. The total heat transfer is divided in an appropriate fashion between the unburned and burned zone. The heat transfer to the burned zone is assigned in total to the boundary zone [**28**].

A linear temperature distribution is assumed for the boundary layer between the wall temperature and adiabatic zone gas temperature [**28**]. In terms of wall temperature and adiabatic zone gas temperature, the average boundary layer temperature, T_{bl} can be defined as,

$$T_{bl} = \frac{T_a - T_{wall}}{\ln(T_a / T_{wall})} \tag{1}$$

where,

T_a = adiabatic core zone gas temperature

T_{wall} = wall temperature

The rate of mass entrainment of the boundary layer is dictated by the mass and energy conservation relations (discussed in the sub-sections) for the adiabatic and boundary layer zones with the above temperature definition.

The mass fraction of the charge within the cylinder which has burned at a given crank angle is specified by a Weibe function of the following form [**29**] shown in eq. (2).

$$x = 1 - e^{-a\left[(\theta-\theta_0)/\Delta\theta_b\right]^{m+1}} \tag{2}$$

where,

x = fraction of the total combusted mass in the cylinder

a = efficiency parameter

m = form factor

θ = crank angle

θ_o = start of combustion

$\Delta\theta_b$ = combustion duration

Eq. (2) is also applicable to the extended thermodynamic model. But for the extended model combustion is terminated when 'x' reaches a value equal to fuel fraction burned. Therefore x_{max}= fuel fraction burned.

4.1.3 Definitions

The following definitions will be used repeatedly in discussing the simulation output. For convenience, definitions have been grouped together in this section.

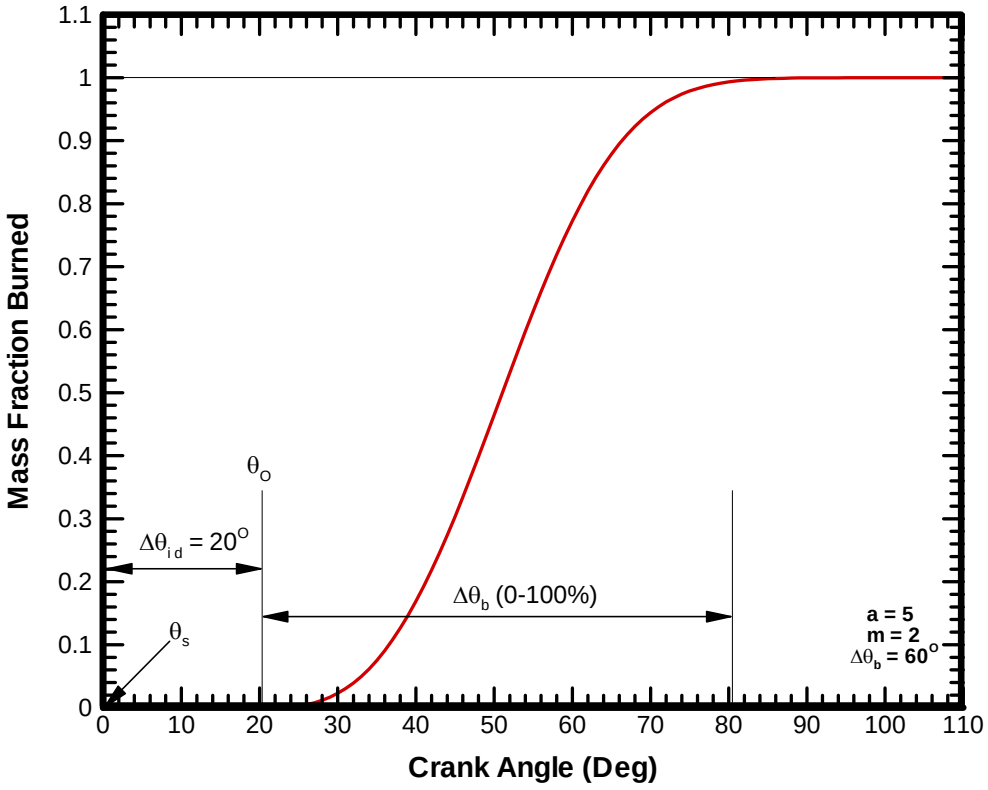

Fig. 3 Schematic of mass fraction burned profile

i) Start of Combustion (θ_o)

The crank angle corresponding to the start of combustion (θ_o) needs to be specified as an input. For $\theta > \theta_o$, the mass fraction burned is given by the Weibe

function, eq. (2). The start of combustion is related to the spark timing by an ignition delay ($\Delta\theta_{id} = \theta_o - \theta_s$, where θ_s is the spark timing), as shown in the Figure 3.

ii) Combustion Duration ($\Delta\theta_b$)

The combustion duration ($\Delta\theta_b$) is specified as an input. This is the crank angle interval from start of combustion (θ_o) to the 100 percent burned position of the curve in Figure 3.

iii) Indicated Performance and Emissions Parameters

The conventional definition of net indicated mean effective pressure (imep) is used; i.e., the values are computed by integrating over the compression and the expansion strokes of the four-stroke cycle. In parametric studies where load is held constant, it is brake mean effective pressure (bmep) which is fixed in value. Total friction mean effective pressure is computed for each operating condition.

iv) Mean Exhaust Temperature (T_{exh})

For each calculation, a mean exhaust temperature is computed by use of the following equation [**30**]:

$$\bar{h}_{exh}(\bar{T}_{exh,} P_{exh}) = \frac{\int_{\theta_{EVO}}^{\theta_{EVC}} \dot{m}\, h_{ev} \frac{d\theta}{360N}}{\int_{\theta_{EVO}}^{\theta_{EVC}} \dot{m}\, \frac{d\theta}{360N}} \qquad (3)$$

where,

$\dot{m}$ = instantaneous mass flow through the exhaust valve

$\bar{h}_{exh}$ = mass average enthalpy at exhaust

P_{exh} = exhaust manifold pressure

h_{ev} = instantaneous enthalpy of gases exiting the cylinder

N = engine speed

The calculated values of T_{exh} may be higher than the typical measured exhaust gas temperatures because heat losses to the exhaust valve, in the exhaust port and in the exhaust manifold, during the exhaust process are not included in the computed value [**30**].

v) Percentage of EGR

The percentage of EGR for this work is defined as:

$$\text{EGR} = \frac{m_{EGR}}{m_{inlet}} \times 100\% \tag{4}$$

where,

m_{EGR} = mass of the exhaust gas recirculated per cycle, and

m_{inlet} = total mass (EGR + air + fuel vapor + residual gas) per cycle that enters the engine.

vi) Fuel Fraction Burned

The other parameter used for this study, Fuel Fraction Burned is defined as:

$$FFB = \left(\frac{m_{\text{fuel burned at comb. termination}}}{m_{\text{total fuel}}} \right)_{cycle} \tag{5}$$

where,

$m_{\text{fuel burned at comb. termination}}$ = mass of fuel burned during a cycle when combustion is terminated.

$m_{\text{total fuel}}$ = total mass of fuel that enters in the cylinder in a cycle.

Any residual gases retained in the cylinder are additional sources of burned gas, are automatically included in the computations, and vary with each operating condition.

4.1.4 Method of Solution

The intake and exhaust processes are based on equations for one-dimensional, quasi-steady flow that are corrected by an empirical discharge coefficient. The intake and exhaust manifolds are assumed to be at constant pressures. The instantaneous valve lift is approximated with a sinusoidal shape based on valve timings and maximum valve lift.

The basic simultaneous differential equations which need to be integrated to simulate the engine cycle are [**30**]:

A) Gas Exchange and Compression Processes
   i) Energy conservation for the cylinder contents.
   ii) Mass flow rate equations for intake and exhaust valves.
   iii) Woschni's correlation for the heat transfer to the walls.

B) Combustion and Expansion Processes
   i) Energy conservation equations for unburned adiabatic core and boundary layer systems.
   ii) Mass burn rate equation.
   iii) Woschni's correlation for heat transfer to the walls for burned and unburned systems.
   iv) Equations for the rate of change of the mass of nitric oxide in the adiabatic core and boundary layers.

These equations are solved using a modified Euler predictor-corrector technique [**30**]. This integration scheme is adequate for solving a system of thermodynamic equations. The NO_x equations are solved using a fourth order predictor-corrector scheme. This added complexity is necessary for accurate integration of the governing equation for NO_x, since the NO_x kinetics is extremely temperature dependent.

Energy Equations

For the compression, late expansion, and exhaust processes, a one-zone formulation is appropriate. The first law of thermodynamics for the one-zone formulation for this system is,

$$\frac{d(mu)}{d\theta} = \dot{Q} - pd\dot{V} + \dot{m}_{in}h_{in} - \dot{m}_{out}h_{out} \tag{6}$$

This equation may be used to find an explicit relation for the derivative of the overall average cylinder gas temperature and cylinder pressure.

As stated previously, for the combustion process, multiple zones are used (see Figure 2). First, the formulation is developed for two zones: an unburned zone and a burned zone. Then, the formulation is extended such that the burned zone may be divided into an adiabatic core zone and a boundary layer zone. The burned zone entrains mass from the unburned zone as the flame front proceeds.

The equations (7) and (8) represent the energy equations for the burned zone and unburned zone, respectively.

$$\frac{d(mu)_b}{d\theta} = \dot{Q}_b - p\dot{V}_b + \dot{m}_b h_b \tag{7}$$

$$\frac{d(mu)_u}{d\theta} = \dot{Q}_u - p\dot{V}_u + \dot{m}_u h_u \tag{8}$$

where, the properties with subscript '*b*' correspond to the burned gas zone and the properties with subscript '*u*' correspond to the unburned gas zone. From these equations, derivatives for the two temperatures (T_u and T_b), the pressure, and the two volumes may be derived.

The next step is to extend the formulation to divide the burned zone into the boundary layer and adiabatic core zones. Initially, the boundary layer zone has zero mass, and the adiabatic core zone contains burned mass. The boundary layer increases in mass

by entraining mass from the adiabatic core. The rate of mass entrainment of the boundary layer is dictated by the mass and energy conservation relations for the adiabatic and boundary layer zones with the above temperature definition. In other words, a specific boundary layer mass is required to satisfy the energy and mass conservation relations. All the burned gas heat transfer is assigned to the boundary layer.

For these additional two zones, the formulation of the energy equation is similar to the above for the overall system. The first law equations for the adiabatic and boundary layer zones, respectively, are:

$$\frac{d(mu)_a}{d\theta} = -p\dot{V}_a + \dot{m}_b h_u - \dot{m}_{bl} h_a \tag{9}$$

$$\frac{d(mu)_{bl}}{d\theta} = \dot{Q}_b - p\dot{V}_{bl} + \dot{m}_{bl} h_a \tag{10}$$

where, properties with subscript '*a*' correspond to the adiabatic core zone and properties with subscript '*bl*' correspond to the boundary layer zone.

Several items, like the thermodynamic properties, mass fraction burned, convective heat transfer, and mass flow rates, are needed to solve the resulting governing differential equations. Finally, a numerical technique is selected to integrate these equations.

The thermodynamic analysis can be used to obtain the governing differential equations for the gas temperatures, the cylinder pressure, the volumes, and the masses. There is a number of numerical methods available to solve a set of differential equations. Both a Runge-Kutta technique and an Euler technique were evaluated. Both of the methods provided surprisingly similar results in terms of final values and execution times. But the application of the Euler technique was more straightforward, and therefore it was selected for this work.

The boundary conditions for the inlet (temperature and pressure) and for the exhaust (pressure) are specified to complete the required input information. Several

parameters are not known at the start of a particular engine cycle simulation. In this case, the initial amount of exhaust gases (residual), and the initial cylinder gas temperature and pressure must be assumed. The complete calculation is repeated until the final values agree with the initial values. Depending on the specified tolerance, this procedure usually finds convergence within about three (3) complete cycles.

The simultaneous numerical integration of the various differential equations is used to obtain the instantaneous cylinder conditions (temperatures, pressure, volumes, masses, and thermodynamic properties) as a function of crank angle. During the combustion process, an iterative approach was needed to solve a number of the differential equations, which are themselves dependent on the other variables. To accomplish this iteration, first the differential equations were evaluated, and then the values from this evaluation were used to determine an updated set of values for the derivatives. This process could be repeated until convergence was obtained. Two iterations were sufficient for convergence for the two-zone model. For the three-zone model, four iterations were necessary.

Heat Transfer

The overall heat transfer $\dot{Q}_{total}$ is based on the cylinder average gas temperature (T_{avg}), and the total surface area (A). The overall heat transfer to the cylinder gases is given by eq. (11).

$$\dot{Q}_{total} = h_c A(\theta)(T_{wall} - T_{avg}) \tag{11}$$

The total heat transfer is allocated to the various zones (but the total is still given by eq. (11)) during the combustion process. A number of ways may be employed to complete this allocation. For this work, the heat transfer is assumed to be proportional to the surface area of each zone. The appropriate surface area of each zone is assumed to be proportional to the zone's volume raised to the 2/3 power. In addition, the heat transfer is proportional to the temperature difference. For example, since the unburned zone

temperature is lower, the proportion of the heat transfer allocated to the unburned zone should be lower as well. This results in the following for the individual allocated heat transfer values,

$$\dot{Q}_u = \left(\frac{V_u}{V_{total}} \right)^{2/3} \left(\frac{T_{wall} - T_u}{T_{wall} - T_{avg}} \right) \dot{Q}_{total} \tag{12}$$

$$\dot{Q}_b = \dot{Q}_u - \dot{Q}_{total} \tag{13}$$

The burned zone heat transfer is assigned in total to the boundary layer zone, because the burned zone is divided into an adiabatic core zone and a boundary layer zone.

To determine instantaneous convective heat transfer coefficient (h_c), a number of correlations have been proposed and used throughout the years. The correlation proposed by Woschni [**27**] has been used in the present work.

Friction

Engine friction losses are typically divided into three main categories: mechanical or rubbing losses, pumping losses, and auxiliary component losses.

a) Mechanical friction can be divided into three component groups,
    1. Crankshaft- main bearings, front and rear main bearing oil seals.
    2. Reciprocating– connecting rod bearings, piston skirts, and piston rings.
    3. Valvetrain– camshafts, cam followers, and valve actuation mechanisms.
b) Auxiliary Losses

    oil pump, water pump, and alternator.
c) Pumping Losses

    intake system, intake and exhaust ports and valves, and exhaust system.

In addition, the exhaust pressure is determined. Algorithms for each of these items were published by Sandoval and Heywood [**32**], and these are used here exactly as presented.

Nitric Oxide Computations

For computing nitric oxides in engines, the extended Zeldovich mechanism for thermal nitric oxides is well accepted [**29**]. Nitric oxides may be formed through one, two or all of the following reactions at the time of combustion.

$$O + N_2 \rightleftarrows NO + N \tag{14}$$

$$N + O_2 \rightleftarrows NO + O \tag{15}$$

$$N + OH \rightleftarrows NO + H \tag{16}$$

An explicit expression may be derived for the change in nitric oxide concentration. For the current study, the nitric oxide kinetics recommended by Dean and Bozzelli [**33**] are used. The kinetics was used as recommended, without employing any adjustments. Caton [**34**] discusses the selection of appropriate nitric oxide kinetics, and provides comparisons of several sets of kinetics. Examples of other nitric oxide computations using isooctane-air mixtures are available from Caton [**35, 36**].

Second Law Parameters

Entropy Balance

The second law analysis may be completed once the final cycle thermodynamics are determined. For any portion of the cycle, an entropy balance may be constructed. In general, the balance is

$$\Delta S = S_{end} - S_{start} = S_{in} - S_{out} + S_Q + \sigma \tag{17}$$

where,

S_{end} = total entropy at the end of the period

S_{start} = total entropy at the start of the period

S_{in} = total entropy transferred into the system

S_{out} = entropy transferred out of the system

S_Q = entropy transferred with the heat transfer process

σ = the total entropy generated by any internal irreversibilities

The entropy transferred into the system with any heat transfer, S_Q (defined positive into the system) is given by,

$$S_Q = \int \frac{\dot{Q}}{T}\, dT \tag{18}$$

where, T = temperature on the boundary of the system where the heat transfer, $\dot{Q}$ occurs.

For the single-zone portion of the simulation, this may be replaced with the system temperature, T_{avg}. For the multiple-zone portion of the simulation, this temperature would be either the unburned gas temperature (T_u) or the burned gas temperature (T_b).

The use of constant temperatures for each zone is consistent with the scope of the current work which includes the transfer of availability due to heat transfer. The destruction of availability associated with heat transfer is related to the temperature at which the energy is received. This final step is outside the defined system for the current work. Further discussion of this topic is available elsewhere [**34**].

The terms S_{in} and S_{out} are given by

$$\begin{aligned} S_{in} &= \int \dot{m}_{in} s_{in}\, dt \\ S_{out} &= \int \dot{m}_{out} s_{out}\, dt \end{aligned} \tag{19}$$

where,

s_{in} and s_{out} = specific entropy flowing in and out respectively.

The entropy generated by irreversibilities will be obtained from the entropy balance given by eq. (17):

$$\sigma = S_{end} - S_{start} - S_{in} + S_{out} - S_Q \tag{20}$$

Availability Parameters

The available energy, also called exergy, of the fuel and the cylinder gases is described by a number of parameters. A brief summary of these parameters is discussed in this section. Full details are available elsewhere [**35**].

The determination of availability is fairly straightforward if the thermodynamic properties are known for a given set of conditions. The kinetic and potential energies can be shown to be negligible, and they are neglected in the present study. At all times, for each zone:

$$a = (u - u_o) - (-p_o(v - v_o)) - T_o(s - s_o) \tag{21}$$

where,

a = specific availability (or exergy for closed systems)

u, v, and s = specific internal energy, the specific volume, and the specific entropy, respectively

u_o, v_o and s_o = specific internal energy, specific volume and specific entropy for the restricted dead state, respectively

p_o *and* T_o = pressure and temperature of the dead state, respectively

The dead state is defined as the conditions of the environment at a temperature of T_o and a pressure of p_o. The term $(-p_o(v-v_o))$ represents the work completed against the atmospheric pressure, p_o and hence not useful[2].

For the open system, the flow availability (or exergy for flows), $a_{f,}$ is given by:

[2] The negative sign for the term "$p_o\,(v-v_o)$" accounts for the fact that as the volume expands ($v<v_o$), the work is done by the system and should be positive.

$$a_f = (h - h_o) - T_o(s - s_o) \tag{22}$$

where,

h = specific enthalpy,

h_o and s_o = specific enthalpy and specific entropy of the restricted dead state, respectively

s = specific entropy of the flowing matter.

For flows into the system, the flowing matter must be specified, and for flows out of the system, the flowing matter is the cylinder contents.

Availability may be destroyed by irreversibilities such as heat transfer through a finite temperature difference, combustion, friction, or mixing processes as availability is not a conserved property. Therefore, the change in the availability may be related to the relevant processes between the given end states:

$$\begin{aligned} \Delta A &= A_{end} - A_{start} \\ \Delta A &= A_{in} - A_{out} + A_Q - A_W - A_{dest} \end{aligned} \tag{23}$$

where,

ΔA = change of the total system availability for a process

A_{end} = total availability at the end of the period

A_{start} = the total availability at the start of the period

A_{in} = total availability transferred into the system accompanying flow into the system

A_{out} = availability transferred out of the system accompanying flow out of the system

A_Q = availability transferred accompanying the heat transfer

A_W = availability transfer due to work

A_{dest} = destroyed availability by irreversible processes

This relation may be used to ascertain the destruction of availability by solving eq. (23) to find A_{dest}. That is,

$$A_{dest} = A_{start} - A_{end} + A_{in} - A_{out} + A_Q - A_W \tag{24}$$

For work interactions, the availability is equal to the useful work (the actual work done minus the work done against the surroundings):

$$A_W = W - W_{surr} \tag{25}$$

where, W_{surr} is the work done against the surroundings and it is given by eq. (26).

$$W_{surr} = p_0(V_{end} - V_{start}) \tag{26}$$

For heat transfer, the availability which is transferred out of the system is equal to the "available" portion of the heat transfer:

$$A_Q = \int \left(1 - \frac{T_o}{T}\right) \delta Q \tag{27}$$

where,

A_Q = available portion of the heat transfer

δQ = differential heat transfer which is transferred at a system (boundary) temperature of T.

The availability that transfers into the system (A_{in}) and out of the system (A_{out}) due to flows is given as follows:

$$\begin{aligned} A_{in} &= \int (\dot{m}_{in}\ a_{f,in})dt \\ A_{out} &= \int (\dot{m}_{out} a_{f,out})dt \end{aligned} \tag{28}$$

where,

$a_{f,in}$ and $a_{f,out}$ = specific flow availability in and out respectively.

For determining the engine efficiency, and for completing the energy and availability balances, values are needed for the energy and availability of the fuel. For the fuel, the lower heating value (*LHV*) evaluated for a constant pressure process is used. By definition, the fuel availability is given by the Gibbs free energy

$$A_{fuel} = -(\Delta G)_{T_o, p_o} \tag{29}$$

For the present study, the fuel used was isooctane. The ratio of the Gibbs free energy and the heating value for isooctane is,

$$\frac{-A_{fuel}}{-LHV} = \frac{(\Delta G)_{T_o, p_o}}{(\Delta H)_{T_o, p_o}} = 1.0286 \tag{30}$$

This ratio, 1.0286, is used to determine the value of the fuel availability by multiplying this number with the fuel's heating value:

$$A_{fuel} = 1.0286 \times (LHV) \times m_f \tag{31}$$

4.2 Extension of Previous Thermodynamic Model

As stated earlier, one of the tasks was to extend the previous thermodynamic simulation to predict engine performance parameters and other results for the use of EGR considering the combustion instability effects at higher EGR levels. To satisfy this objective, two parameters were selected which could be shown to be affected by increasing EGR rate. Several trials were made with each of the selected parameters.

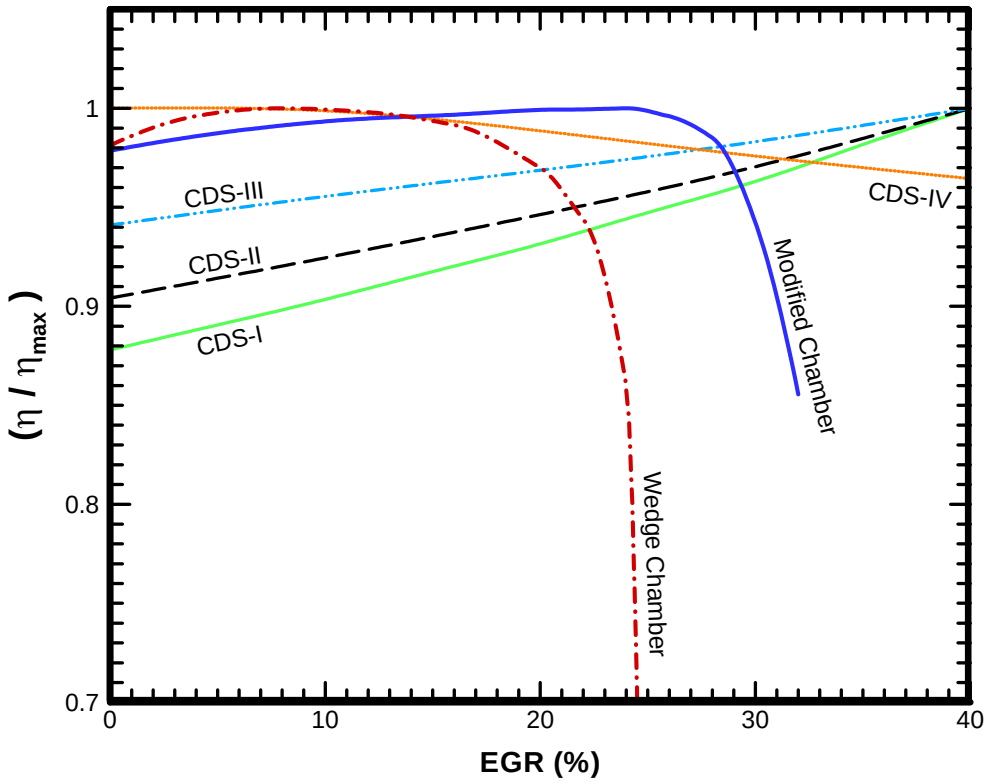

Fig. 4 Plot of efficiency ratio, (η/η_{max}) as functions of EGR percentage for four different combustion duration schedules and for experimental results (for modified chamber and wedge chamber) for cooled EGR configuration

Considering the fact that slow burn cycles appear first as EGR level increases, the first parameter chosen for the trials was the combustion duration ($\Delta\theta_b$). Several combustion duration schedules as a function of EGR percentage were tried for both cooled and adiabatic EGR configurations. The combustion duration was increased as the EGR level was increased for each of the combustion duration schedules. This is due to the reason that frequency of slow burn cycles increases rapidly as EGR level increases. The efficiency trend of each of the trials was compared with the experimental efficiency trend [**4**]. The absolute values of thermal efficiencies, from the simulation, may be quite different from the experimental efficiency values, since the experiments [**4**] were

performed to compare the thermal efficiency of two different combustion chamber designs (modified chamber and wedge chamber, see Figure 1) as a function of EGR level, and in the present study, the simulation used a cylindrical shaped combustion chamber design for simplicity. Therefore, to compare the efficiency trends, the efficiency ratio, (η/η_{max}) vs. EGR percentage for different combustion duration schedules (CDS-I, II, III, & IV), and for experiment results were plotted on the same plot, and it is shown in Figure 4[3].

None of the combustion duration schedules resulted in the efficiency trend that could be a close approximation to the experimental efficiency trends (Figure 4). The details of all the combustion duration schedules and the corresponding efficiency trends (absolute values of efficiencies) are given in Appendix.

At about 20% EGR rate partial burn cycles start to appear and misfire cycles appear at approx. 24% EGR [**10,** see Figure 29]. To catch the effects of partial burn and misfire, a parameter called Fuel Fraction Burned was introduced as a part of second set of trials. Different fuel fraction burned schedules like constant, linear, combination of constant and linear, quadratic and third order polynomial (see Appendix for details) were chosen for trials. Fuel fraction burned schedule gives a specific value of fraction of fuel (between 0 and 1) that would burn under the given EGR level.

The efficiency results with each FFB schedule were compared with the experimental results. As stated above, to compare the efficiency trends, the efficiency ratio, (η/η_{max}) vs. EGR percentage for different FFB schedules (FFBS-I, II, III, IV, & V) and for experiment results were plotted on the same plot, and it is shown in Figure 5.

---

[3] Figures 4 and 5 show the efficiency ratio, (η/η_{max}) vs. EGR percentage plots for cooled EGR configuration only, since the absolute efficiency values for both cooled and adiabatic EGR configurations are very close. The detailed results for both configurations are given in Appendix.

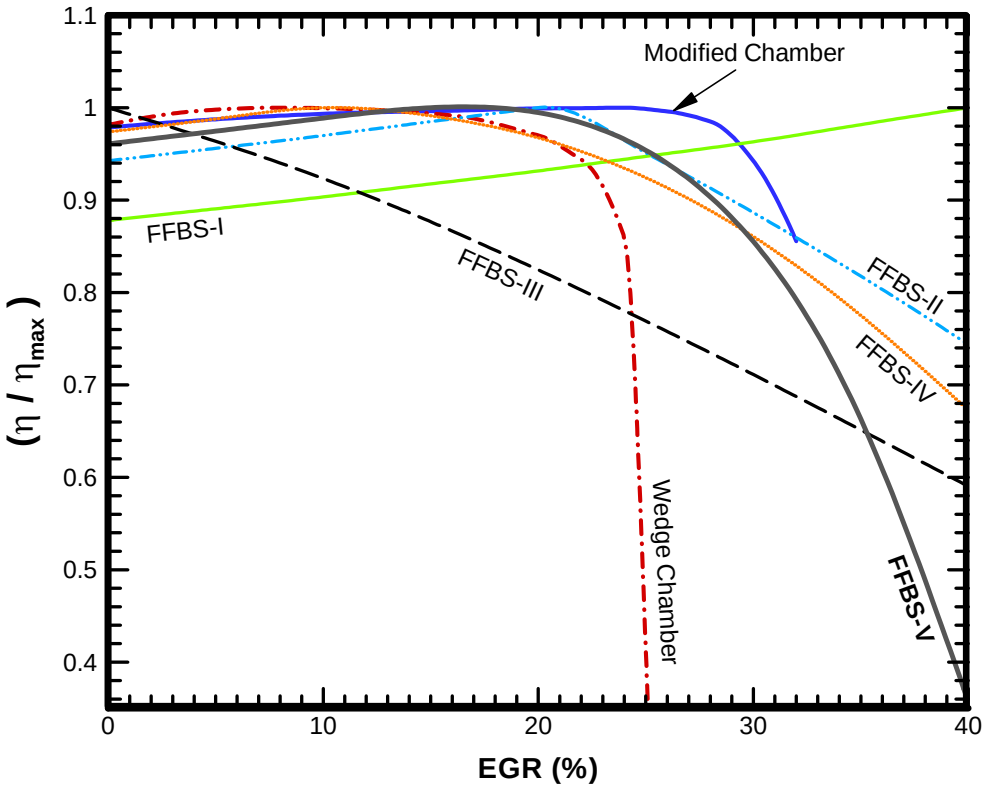

Fig. 5 Plot of efficiency ratio, (η/η_{max}) as functions of EGR for five different fuel fraction burned schedules and for experimental results (for modified chamber and wedge chamber) for cooled EGR configuration

As shown in Figure 5, out of all the FFB schedules tried, the FFBS-V (given by eq. (32)) gave the best fit with experimental results [**4**], and it is shown in Figure 6.

$$\text{FFB} = 1 - \left[\left(\frac{76}{3}\right)\times\left(\frac{\text{EGR}}{100}\right)^{3}\right] + \left[\left(\frac{19}{3}\right)\times\left(\frac{\text{EGR}}{100}\right)^{2}\right] - \left[\left(\frac{12}{25}\right)\times\left(\frac{\text{EGR}}{100}\right)\right] \qquad (32)$$

where, EGR = Percentage of exhaust gas recirculated. The details of all the FFB schedules and the corresponding efficiency trends (absolute values of efficiencies) are given in Appendix.

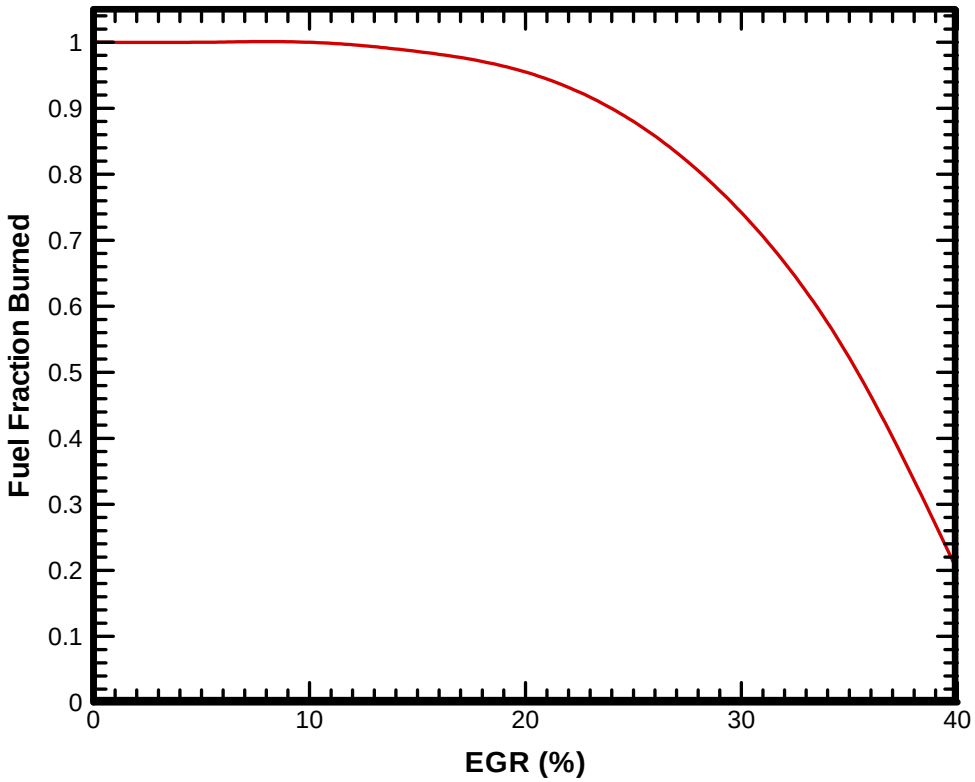

Fig. 6 Fuel fraction burned as functions of EGR percentage

Finally the previous thermodynamic model was modified to include FFB as one of the input parameters and to reflect its subsequent effects on combustion, emissions, heat transfer, temperatures etc.

With this FFB in effect at a given EGR level, the new mass fraction burned at any given crank angle is same as that defined by the Weibe function (eq. (2), Figure 3) except the combustion is terminated when the mass fraction burned reaches the FFB value ($x_{\max} = \mathrm{FFB}$). Figure 7 shows the schematic of mass fraction burned profile with the FFB (=0.88, calculated from eq. (32)) corresponding to 25% EGR.

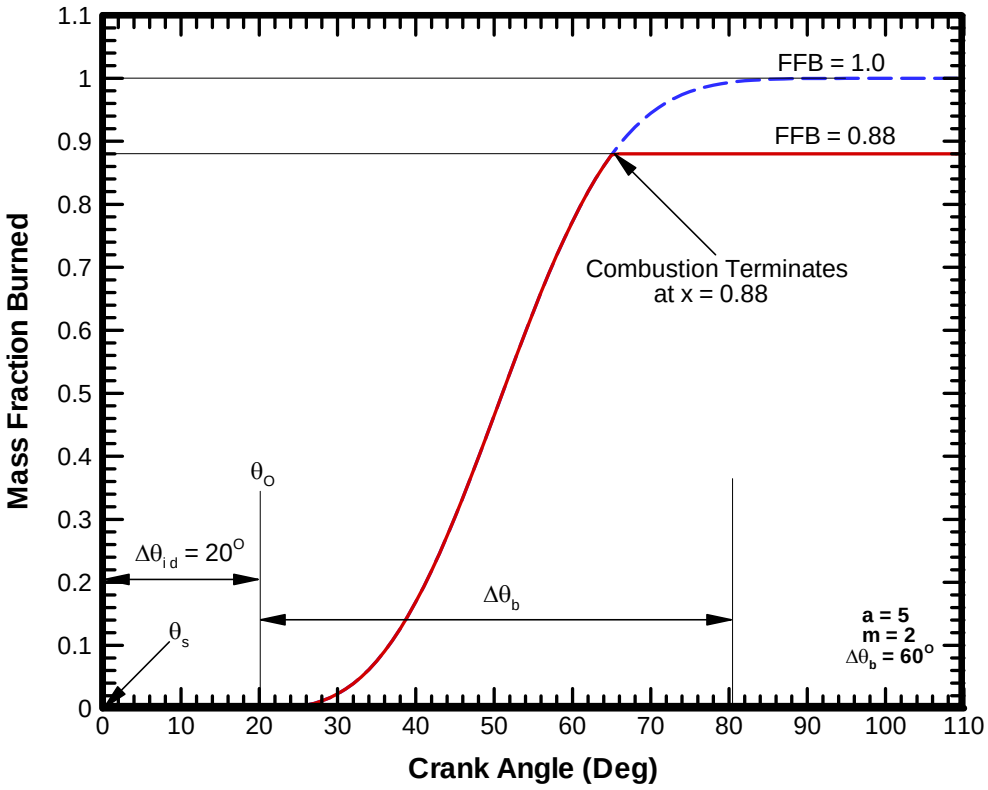

Fig. 7 Schematic of mass fraction burned profile with FFB = 0.88 at 25% EGR

5. RESULTS AND DISCUSSION

The results from this study are preceded by a brief discussion of the limitations of this study, specifications of engine used for the study, a brief description of the study methodology, and a brief presentation of the relevant thermodynamic property results. These preliminary sub-sections are followed by the majority of the results presented in two main sub-sections: (1) constant load and speed results, and (2) variable load and speed results.

5.1 Limitations of the Study

As already discussed in one of the earlier sections, cyclic variations in the combustion process are caused by variations in mixture motion within the cylinder at the time of spark cycle-by-cycle, variations in the amounts of air and fuel fed to the cylinder each cycle, and variation in the mixing of fresh mixture and residual gases within the cylinder each cycle, specifically in the vicinity of the spark plug. Variations between cylinders are caused by differences in these same phenomena, cylinder-to-cylinder. It is very difficult to capture the above mentioned aspects of combustion process in the simulation work. Therefore, the following computations did not consider cycle-by cycle variations. Also, the present simulation did not consider the possibility of spark knock or preignition.

Apart from this, during the actual engine operating cycles gas flows into and out of the small volumes (connected to combustion chamber), usually called ‘crevices’, as the cylinder pressure changes. The volumes between the piston, piston rings, and cylinder wall are the largest crevices. Blow by is the gas flow out of these regions in to the crank case. The present calculations assumed the blow-by to be zero.

For conventional SI engines, the maximum EGR level is typically limited to about 15-20%. At higher levels of EGR, the combustion stability becomes an issue as combustion patterns, which are responsible for unstable engine operation, start to appear at a very high frequency. A relatively wide range of EGR levels is considered in this

study to better illustrate the trends with respect to increases of EGR. This higher level of EGR may or may not be practical in actual application.

5.2 Difference between Cooled and Adiabatic EGR Configurations

In the "cooled" EGR configuration, the EGR gases are cooled to the inlet air-fuel temperature before they are mixed with the inducted charge of air-fuel, whereas in the "adiabatic" EGR configuration, no cooling is used and the EGR gases maintain their engine exit temperature. For the adiabatic EGR configuration, the EGR gases mix adiabatically with the inducted charge of air-fuel. This mixture enters the engine with the temperature consistent with the energies of the two streams depending on the amount of EGR.

Table 3 Engine specifications

Item	Value
Number of Cylinders	8
Bore (mm)	101.6
Stroke (mm)	88.4
Crank Radius/Con Rod Ratio	0.305
Compression Ratio	8.1:1
Inlet Valves:	
Diameter (mm)	50.8
Max Lift (mm)	10.0
Opens (^{o}CA aTDC)	357
Closes (^{o}CA aTDC)	-136
Exhaust Valves:	
Diameter (mm)	39.6
Max Lift (mm)	10.0
Opens (^{o}CA aTDC)	116
Closes (^{o}CA aTDC)	371
Valve Overlap (degrees)	14^{o}
Heat Transfer Multiplier	1.33

5.3 Engine Specifications

A 5.7 liter, V-8 configuration automotive engine with a compression ratio of 8.1:1 and with a bore and stroke of 101.6 and 88.4 mm, respectively was selected for the present study. This engine was used in a series of previous studies (e.g. [**21, 25, 28, 34-37**]). Table 3 lists the engine specifications as used in the present work.

5.4 Study Methodology

The following section illustrates the methodology for conducting the parametric study. First a set of operating conditions are selected which are representative of the typical conditions and these conditions, therefore, define the base case for the parametric study. Then a structure consisting of the variables selected for conducting the parametric study is formed.

5.4.1 Operating Conditions

Ordinary spark ignition engine operation encompasses a wide range of operating modes, e.g., idle, acceleration, deceleration, and cruise. Previous analyses [**30**] suggest that the results of a parametric study are most useful if the engine speed and load are held constant at some selected values which are representative of the typical operating modes. Therefore, for the present study, a moderate vehicle acceleration point for engine speed of 1400 rpm and brake torque of 149 N-m (110 lb-ft), which generates a bmep of around 325 kPa, was chosen as the primary reference point.

In addition to the primary study with the use of EGR (load and speed were kept constant), the engine variables selected for the second part of the study were load (bmep) and engine speed. FFB was varied with EGR percentage as calculated from eq. (32). Also combustion timing was set to give maximum brake torque for each set of operating conditions. The other parameters like compression ratio, equivalence ratio, combustion duration, and cylinder wall temperature were held constant throughout the study. Inlet (air-fuel) temperature was kept constant for cooled EGR configuration whereas for

adiabatic EGR configuration it was computed from energy balance and mass balance equations.

The start of combustion timing which gives maximum brake torque is called MBT combustion timing. MBT start of combustion timing was determined from the plots of bmep vs. θ_o (start of combustion). It was found to be essentially independent of equivalence ratio and percent EGR for a given engine geometry, engine speed and combustion duration [**30**]. To maintain bmep constant at the chosen load-speed point as other parameters are varied, the inlet pressure P_{in} was varied in the simulation input.

Table 4 Various parameters for engine and fuel for the base case

Item	Value Used	How Obtained
Displaced Volume (dm^3)	5.733	computed
AF_{stoich}	15.13	for isooctane [**26**]
Equivalence Ratio, ϕ	1.0	input
Frictional mep (kPa)	68.5	from algorithm
Inlet Pressure (kPa)	50.5	input
Exhaust Pressure (kPa)	102.6	from algorithm
Engine Speed (rpm)	1400	input
Start of Combustion (^{o}bTDC)	20.0	determined for MBT
Combustion Duration (^{o}CA)	60	input
Inlet (air-fuel) Temperature	319.4 K (315^oF)	input
Cylinder Wall Temp (K)	450	input
Fuel LHV (kJ/kg)	44,400	for isooctane [**26**]

5.4.2 Base Operating Conditions

The base operating point for the parametric study was chosen to be at an engine speed of 1400 rpm, load as 325 kPa, ϕ = 1.0, 0% EGR, MBT timing, 60° burn duration, and 8.1:1 as the compression ratio. At this load and speed, the computed value of fmep was 68.5 kPa, while the $imep_{net}$ was 394.0 kPa. The input data for this base case calculation is presented in Table 4. The simulation calculates parameters like cylinder volume, inlet and exhaust mass flow rates, cylinder pressure, mass fraction burned, unburned and burned gas temperatures, nitric oxide concentration, and heat transfer rates as functions of crank angle.

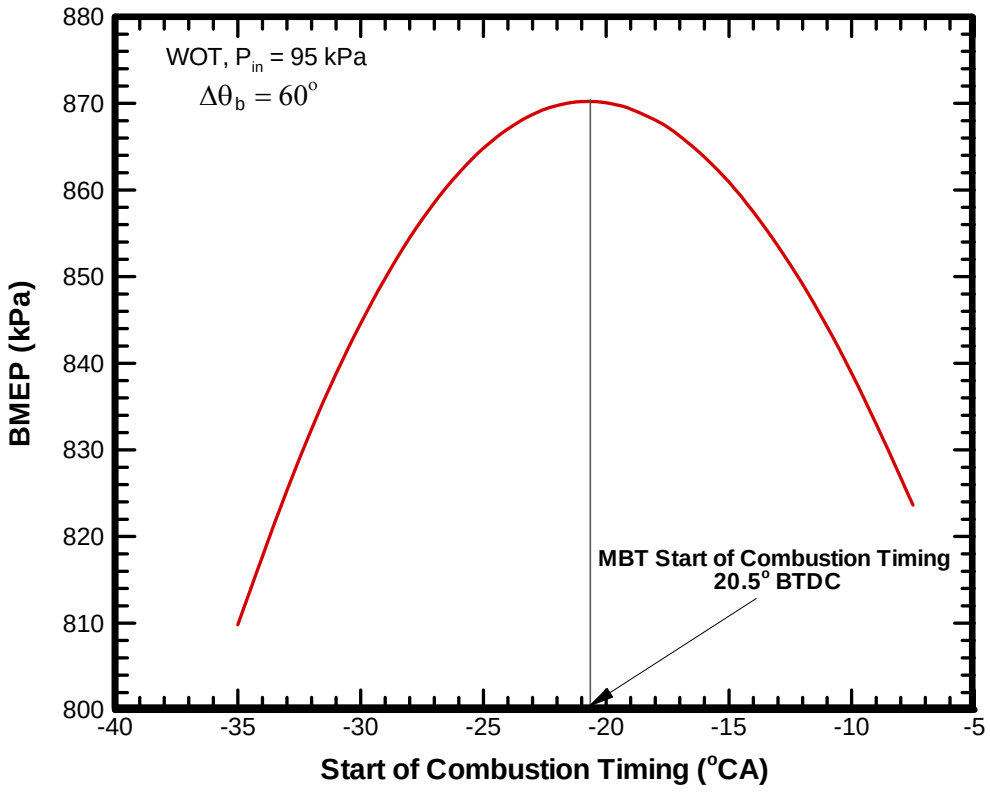

Fig. 8 Plot of bmep as functions of start of combustion timing to determine the optimum timing for the maximum torque

As documented previously, MBT start of combustion timing was determined from the plots of bmep vs θ_o. Figure 8 shows a typical plot for the base case combustion duration of $\Delta\theta_b$=60° for WOT condition (P_{in}=95 kPa). This approach was followed throughout to determine the optimum start of combustion timing.

5.4.3 Strategy of the Study

The primary objective of the present research project was to use a thermodynamic cycle simulation to obtain results for the use of EGR in a spark ignition engine under the consideration of combustion instabilities. As documented in section 4.2, the previous model was extended to include a parameter called Fuel Fraction Burned to incorporate combustion instability effects.

Table 5 Structure of the parametric study for 5.7 liter automotive engine

Para-meters to Vary	**BMEP (kPa)**	**N (rpm)**	**EGR (%)**	**FFB**	**ϕ**	**$\Delta\theta_b$ (^oCA)**	**Start of Comb-ustion Timing**	**r**
EGR	325	1400	0-40	1.0-0.2	1.0	60	MBT	8.1
BMEP	0-WOT	1400	0 & 20	1 & 0.955	1.0	60	MBT	8.1
Speed	325	600-6000	0 & 20	1 & 0.955	1.0	60	MBT	8.1

Once the thermodynamic model was extended to incorporate combustion instability effects, the strategy of the study was (*part 1*) to first determine engine performance as functions of the amount of EGR for a constant load (*bmep* = 325 kPa) and constant speed (1400 rpm), and (*part 2*) then to determine engine performance as

functions of engine loads and speeds for 0% and 20% EGR. Two configurations were examined for the use of EGR: (1) cooled and (2) adiabatic. Both configurations were examined for finalized FFB schedule defined by eq. (32).

In *part 2*, engine performance as functions of engine loads and speeds was determined at 0% and 20% EGR (cooled and adiabatic). From the eq. (32) for 0% and 20% EGR, FFB was 1(one) and 0.955, respectively. As already stated, the "cooled" EGR configuration represents cooling the EGR gases to the air-fuel temperature (319.4 K (115°F) for this study). The "adiabatic" configuration represents the use of no cooling such that the EGR gases maintain their engine exit temperature. For this configuration, the EGR gases then mix adiabatically with the inducted charge of air/fuel (at 319.4 K). This mixture enters the engine with the temperature consistent with the energies of the two streams depending on the amount of EGR. Results for this mixture temperature are given in Table 6. These two EGR configurations result in inlet mixture temperatures that bracket the possible temperatures in practice.

Table 5 lists the organization of the parametric study; in each part of the study all variables was held constant at a base value except for two which are varied over the range shown.

5.5 Basic Thermodynamic Properties

As discussed in the previous section the use of adiabatic EGR alters the inlet temperature of the (EGR + Air + Fuel) mixture, in general whether it is cooled or adiabatic use of EGR alters several aspects of the thermodynamics compared to the use of pure air. These aspects include the increase of species such as nitrogen, carbon dioxide and water vapor in the inlet mixture, the different equilibrium product concentrations in the product gases, and the resulting different thermodynamic properties in both the reactant and product gas mixtures. Also as a large fraction of fuel remains unburned at higher EGR level, product gas mixture also includes unburned hydro-carbons in it.

These changes cause the ratio of specific heats to increase with increases in the EGR level. This is a result of the higher concentrations of species which have higher ratios of specific heats. This increase is greater for the cooled EGR configuration (lower temperatures) than for the adiabatic EGR configuration.

5.6 Results of the Parametric Study

5.6.1 Constant Load and Speed Results

Figure 9 shows the inlet mixture temperatures as functions of the percentage of EGR for the base case for the two EGR configurations. As mentioned above, with no EGR, the inlet air-fuel mixture is assumed to enter the cylinder at a temperature of 319.4 K (115°F). For the cooled configuration, the complete inlet mixture (air, fuel vapor and EGR) temperature is constant (with a value of 319.4 K) as the percentage of EGR increases. For the adiabatic EGR configuration, the inlet mixture temperature first increases, reaches a maximum (at about 24% EGR), and then decreases as the EGR level increases. This is because, for EGR levels between 0 and 24%, the increase of EGR results in a very small fraction of unburned fuel, and hence the exhaust gas temperature is sufficiently high to increase the inlet gas mixture temperature. This effect (increase of inlet mixture temperature) tends to increase the combustion temperatures, but the dilution effect tends to decrease the temperatures. For EGR level between 0% and about 24% the two effects are roughly in balance and the gas temperature does not change much. But beyond 24% of EGR level, the fraction of unburned fuel increases rapidly as EGR level increases and consequently combustion temperatures and exhaust gas temperature decrease rapidly.

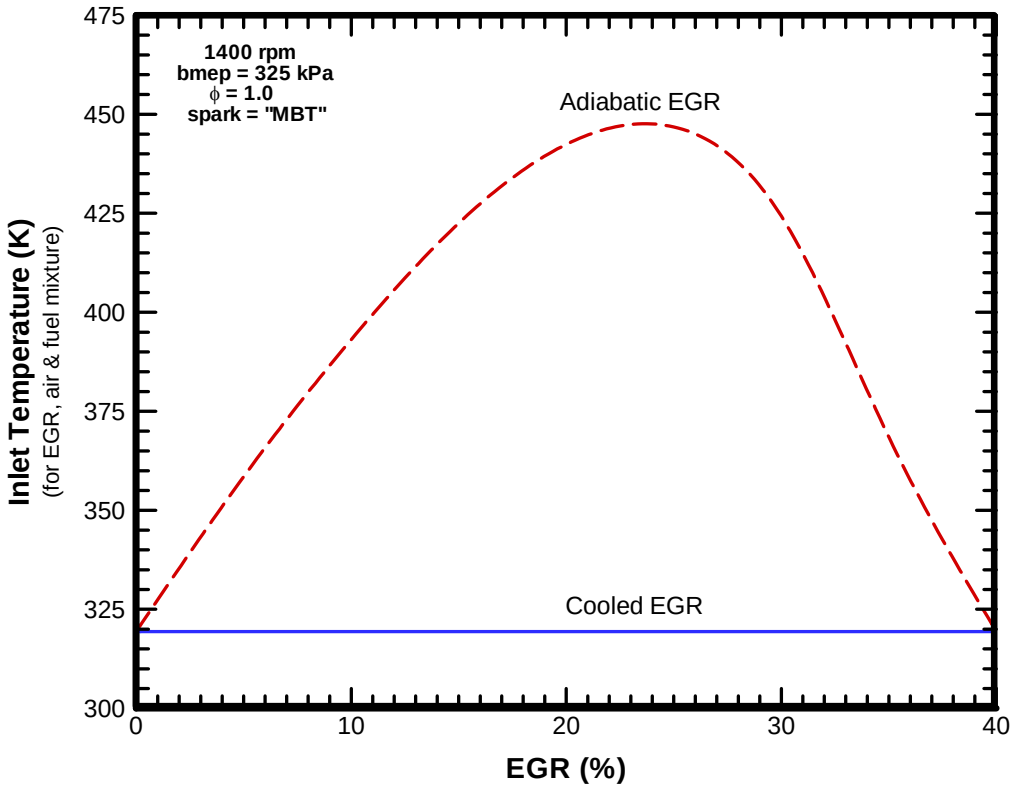

Fig. 9 Inlet mixture temperature as functions of the percentage of EGR for the base case conditions for both cooled and adiabatic EGR configurations

Above 24% EGR, both effects (dilution effect and reduced combustion temperatures due to a large fraction of unburned fuel) tend to decrease the inlet gas mixture temperature. For 24% EGR, the inlet mixture temperature is about 447 K for these conditions.

Tables 6 and 7 are summary lists of some of the relevant input parameters and results for the base case load and speed for no EGR and eight (8) EGR levels. As shown for cooled EGR, as the EGR level increased initially, the start of combustion (θ_o) was kept constant to obtain MBT performance. For adiabatic EGR case, the start of combustion needed to advance from 20^o BTDC to 25^o BTDC when EGR was increased

from 0% to 25%. For both configurations above 25% EGR, the start of combustion needed to retard significantly because FFB decreases rapidly at higher EGR levels.

Table 6 Some parameters as functions of EGR

(1400 rpm, bmep = 325 kPa, ϕ = 1.0)

Item→ Case↓	**EGR (%)**	**Fraction Fuel**	**θ_o (relative to TDC)**	**P_{in} (kPa)**	**P_{exh} (kPa)**	**$T_{in,mix}$ (K)**
No EGR	0	1.000	-20.0	50.5	102.6	319.4
Cooled	5	1.000	-20.0	52.2	102.7	319.4
Cooled	10	1.000	-20.0	54.1	102.8	319.4
Cooled	15	0.985	-20.0	56.4	102.9	319.4
Cooled	20	0.955	-20.0	59.9	103.2	319.4
Cooled	25	0.880	-19.0	65.7	103.5	319.4
Cooled	30	0.742	-18.0	77.0	104.4	319.4
Cooled	35	0.522	-17.5	103.4	106.8	319.4
Cooled	40	0.200	-11.5	237.4	130.1	319.4
Adiabatic	5	1.000	-22.0	56.7	103.0	358.5
Adiabatic	10	1.000	-23.5	62.9	103.3	393.1
Adiabatic	15	0.985	-24.5	69.4	103.8	422.5
Adiabatic	20	0.955	-25.0	76.5	104.3	442.4
Adiabatic	25	0.880	-24.5	85.1	105.0	446.8
Adiabatic	30	0.742	-23.0	96.3	106.1	424.3
Adiabatic	35	0.522	-19.5	120.2	108.7	368.5
Adiabatic	40	0.200	-14.0	239.1	130.5	319.4

The retardation in the start of combustion follows from two effects. As discussed previously as the EGR level increases, slow burn cycles appear first at about 8 % EGR

and frequency of occurrence of slow burn cycles increases rapidly after 25% EGR. Due to slow burn, start of combustion tends to retard.

Table 7 Some results as functions of EGR

(1400 rpm, bmep = 325 kPa, ϕ = 1.0)

Item → **Case↓**	**EGR (%)**	**η_b (%)**	**η_i (%)**	**$T_{avg\ exh}$ (K)**	**$T_{avg\ comb}$ (K)**	**RHT (%)**
No EGR	0	25.34	30.68	1090.4	1615.8	28.55
Cooled	5	25.69	31.12	1047.8	1579.1	27.91
Cooled	10	26.07	31.58	1004.9	1540.9	27.21
Cooled	15	26.31	31.90	954.5	1501.1	26.25
Cooled	20	26.14	31.73	883.6	1455.4	24.58
Cooled	25	25.01	30.43	785.0	1388.3	21.23
Cooled	30	22.32	27.28	640.4	1283.1	16.11
Cooled	35	17.11	21.15	436.2	1115.7	9.25
Cooled	40	8.78	11.40	319.4	874.8	2.64
Adiabatic	5	25.61	31.08	1047.7	1616.3	29.54
Adiabatic	10	25.89	31.48	1008.7	1611.8	30.29
Adiabatic	15	26.04	31.75	965.9	1600.7	30.55
Adiabatic	20	25.81	31.56	903.3	1576	29.68
Adiabatic	25	24.72	30.31	810.6	1518.9	26.59
Adiabatic	30	22.02	27.13	665.1	1396.4	20.42
Adiabatic	35	17.09	21.29	463.2	1188.6	11.64
Adiabatic	40	8.67	11.28	319.4	879.5	2.68

The other effect is of fuel fraction burned which is the representation of combustion stabilities in the present study. At higher EGR levels (above 25%), as EGR percentage increases, FFB decreases (increases unburned fraction of fuel) which means

not all fuel is being burned and theoretically start of combustion is to be retarded from the normal (when 100% fuel burns) start of combustion. At lower EGR levels, as EGR percentage increases, fuel fraction burned decreases slightly and hence start of combustion may not be changed much (for cooled case) or it may be advanced (for adiabatic case). Also as the EGR level increases, the inlet pressure needs to increase to obtain the constant load (bmep=325 kPa). Also, the exhaust pressures increase slightly as the EGR level increases for both cases due to the increased mass flow for the same engine load. The exhaust gas temperatures are higher for the adiabatic EGR configuration, and decrease with increases of the EGR levels. This decrease of the exhaust gas temperature is a direct consequence of the dilution effect of the higher EGR levels as well as combustion patterns causing unstable engine operation (slow burn, misfire and partial burn).

Nitric Oxide Results

To demonstrate the effectiveness of EGR for reducing nitric oxide emissions, Figure 10 shows the nitric oxide concentrations as functions of the percentage of EGR for the base case for the two EGR configurations. The nitric oxide concentration decreases rapidly with increasing EGR. The cooled EGR configuration results in lower nitric oxide emissions relative to the adiabatic EGR configuration since the gas temperatures are lower (described in the next sub-section). Even for the adiabatic EGR configuration, however, over 90% reduction in nitric oxide is obtained with about 26% EGR.

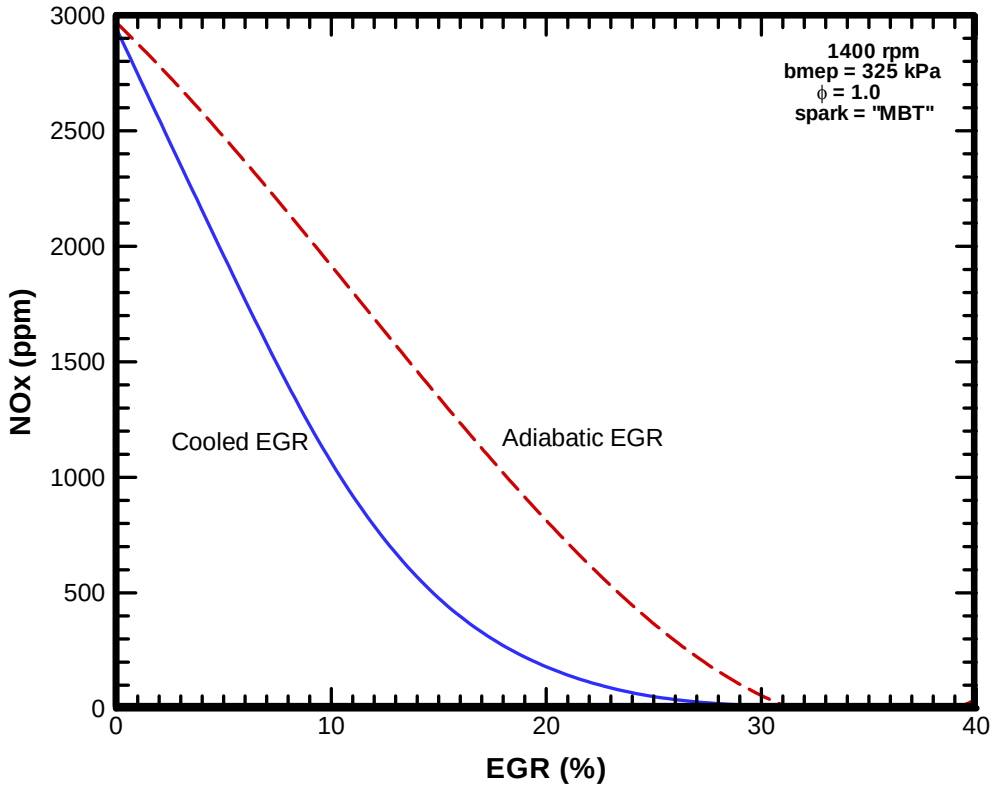

Fig. 10 Nitric oxide concentration in the exhaust as functions of the percentage of EGR for the base case conditions for both cooled and adiabatic EGR configurations

Thermal Efficiencies Results

Figure 11 shows the (*net)* indicated and brake thermal efficiencies as functions of the percentage of EGR for the base case for the two EGR configurations. Both the indicated and brake efficiencies first increase, reach a maximum (at about 16% EGR) and then decrease as EGR level increases, and the results are similar for the two EGR configurations. In general, the brake thermal efficiency is slightly higher for the cooled EGR case. The brake thermal efficiency increases from about 25.3% to about 26.4% as EGR increases from 0 to 16%. These increases of the thermal efficiencies for the use of EGR are the result of lower gas temperatures, lower heat transfer, favorable thermodynamic properties, reduced dissociation near top dead center, and lower

pumping losses (a consequence of the constant load condition). But for greater than 16% of EGR the fuel energy is wasted as a result of incomplete combustion (unburned fuel) caused by excessive EGR and its effect is predominant over the improvement in the efficiency due to the above mentioned factors. The overall result is a reduction in the efficiency as the EGR level increases. These items are quantified in the following discussion. Below, in this report, the reasons for the similar results for the two EGR configurations are explained in terms of the various energy and availability terms.

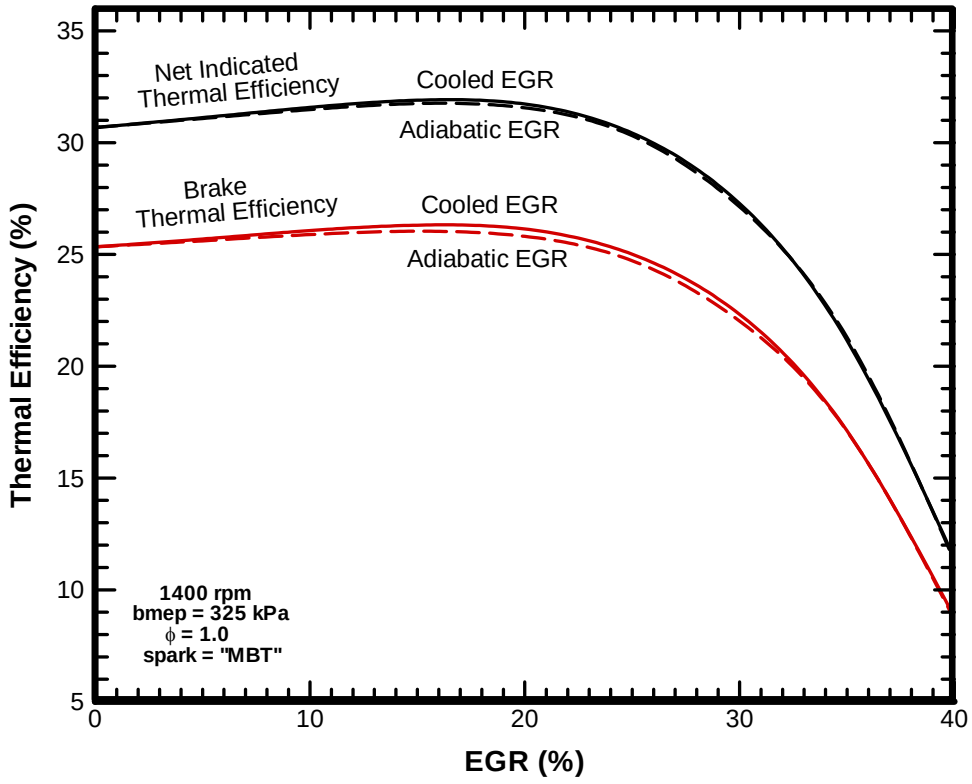

Fig. 11 Indicated and brake thermal efficiency as functions of the percentage of EGR for the base case conditions for both cooled and adiabatic EGR configurations

The results in Figure 11 illustrate an interesting feature of the trade-offs. The cooled EGR configuration has higher gross indicated efficiency largely due to the lower

heat losses relative to the adiabatic case. The adiabatic EGR configuration has lower pumping friction compared to the cooled EGR configuration since the gross indicated efficiency is lower so that the throttle must be more open to obtain the same bmep. These two effects are about equal, and the overall result is that the net indicated efficiencies are about the same for the two EGR configurations.

Temperature and Heat Transfer Results

Figure 12 shows the maximum cylinder gas temperatures, average gas temperatures during the combustion process (θ_o< CA <θ_{end}), and average exhaust gas temperatures (for the exhaust valve open period) as functions of the percentage of exhaust gas recirculation for the base case conditions for both cooled and adiabatic EGR configurations. The maximum cylinder gas temperature was a single (spatial average) temperature that typically occurred at about 22–29^o ATDC (depending on conditions). The average exhaust gas temperatures are based on energy-weighted averages. In general, all three temperatures decrease as the percentage of EGR increases, and the three temperatures are higher for the adiabatic configuration relative to the cooled configuration, as expected. But for EGR levels greater than about 24%, decreases in the three temperatures are much rapid as functions of EGR, and its effect can be seen in the inlet mixture temperature also. This is because of the combustion instability issues (slow burn, partial burn, and misfire) associated with high levels of EGR.

Figure 13 shows the relative heat transfer as functions of the percentage of exhaust gas recirculation for the base case conditions for both the cooled and adiabatic EGR configurations. The relative heat transfer is the ratio of the heat transfer energy and the fuel input energy. For the cooled EGR configuration, the relative heat transfer decreases as the EGR level increases. This is due to the decrease of the gas temperatures as the EGR level increases. The decrease in relative heat transfer is much more rapid above about 24% EGR due to the rapid decrease in temperatures (Figure 12).

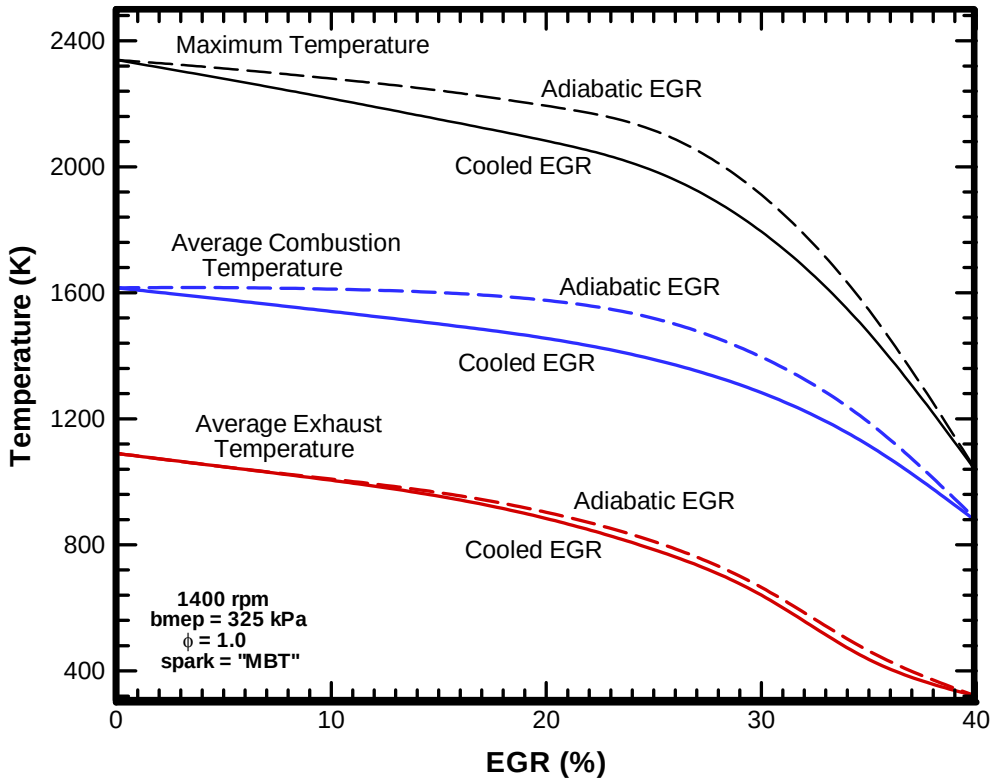

Fig. 12 Maximum cylinder gas temperatures, average gas temperatures during the combustion process, and average exhaust gas temperatures as functions of the percentage of EGR for the base case conditions for both cooled and adiabatic EGR configurations

For the adiabatic EGR configuration, the relative heat transfer first increases, reaches a maximum (at about 16% EGR), and then decreases as the EGR level increases. This is because, for EGR levels between 0 and 24%, the increase of EGR increases the inlet gas mixture temperature as well as providing a dilution effect. The first effect (increase of inlet mixture temperature) tends to increase the combustion temperatures, but the dilution effect tends to decrease the temperatures. For EGR levels between 0% and about 24%, the two effects are roughly in balance, and the gas temperatures do not change much (Figure 12). In addition, the heat transfer coefficient increases slightly as

EGR levels increase[4]. The net effect is that the absolute as well as the relative heat transfer rates increase for EGR levels between 0% and about 16%.

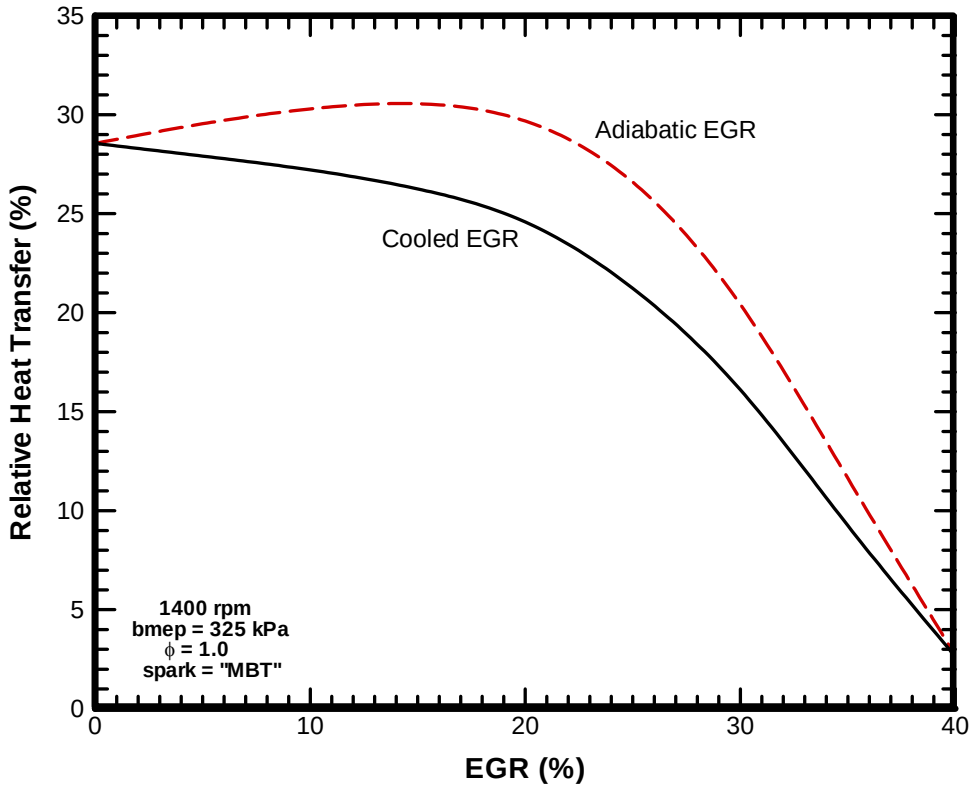

Fig. 13 The relative heat transfer as functions of the percentage of the EGR for the base case conditions for both cooled and adiabatic EGR configurations

For EGR levels greater than about 16%, the dilution effect dominates, and unstable combustion patterns (partial burn and misfire) cause the gas temperatures to decrease as EGR increases. This results in the absolute heat transfer and the relative heat transfer decreasing as the EGR level increases.

[4] The heat transfer coefficient is dependent on the cylinder pressure (to a fractional power) – so, for increasing cylinder pressures (as EGR levels increase), the heat transfer coefficient increases.

Availability Results

Figures 14 and 15 show the four of the five major availability terms as functions of the percentage of EGR for the base case for the cooled and adiabatic EGR configurations, respectively. Figure 16 shows, the fifth availability term which represents the aspect of incomplete combustion in the form of availability of unused fuel. The majority of the availability of the fuel is distributed between these five terms. These results can best be explained by knowing the changes in the various gas temperatures (Figure 12).

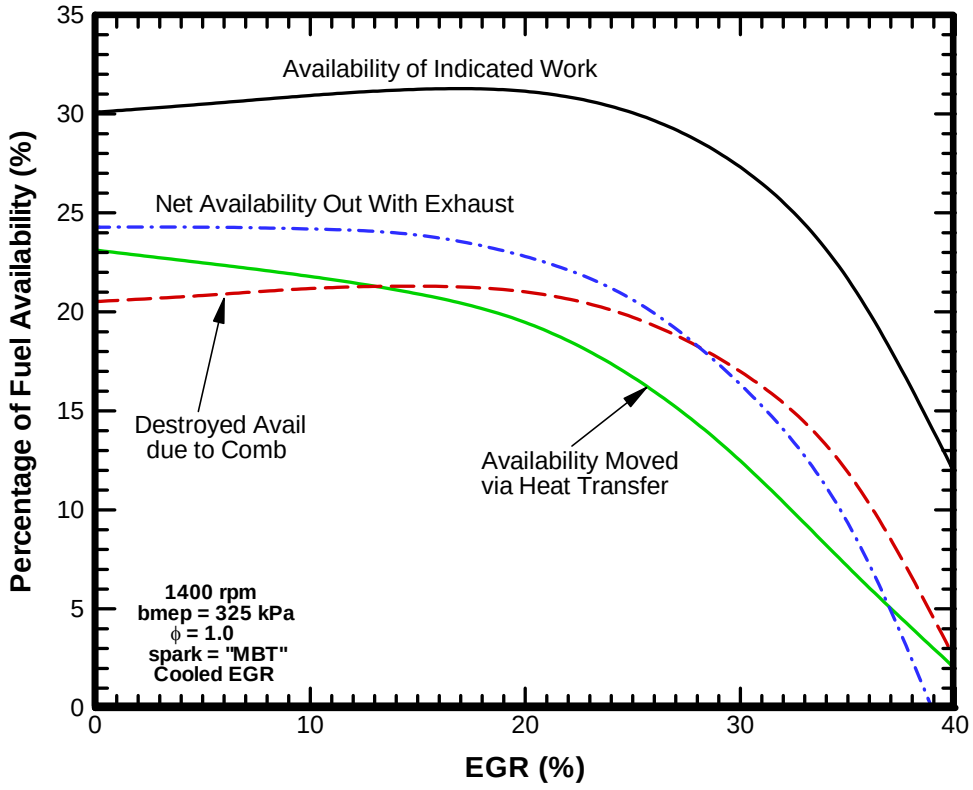

Fig. 14 Four availability terms as functions of the percentage of EGR for the base case conditions for the cooled EGR configuration

For the cooled EGR configuration (Figure 14), the results are fairly straight forward. For this configuration, the availability associated with the indicated work increases slightly as EGR increases from 0 to about 16% EGR. For higher levels of EGR, the availability associated with indicated work starts decreasing due to the effect of incomplete combustion. This is reflected in the indicated thermal efficiency trend (Figure 11). The indicated thermal efficiency increases from 0 to about 16% EGR and then for higher levels of EGR above 16% it starts decreasing (Figure 11). The net availability leaving the cylinder with the exhaust gases refers to the difference between the availability leaving (exhaust) and entering (intake charge). The net availability leaving with the exhaust flow decreases as EGR increases, and this follows from the decrease of the exhaust temperature as EGR increases. The availability moved with the heat transfer to the cylinder walls decreases as EGR increases, and this is a result of the decreasing heat transfer as EGR increases (Figure 13).

For the cooled EGR configuration (Figure 14), the availability destroyed during the combustion process increases slightly as the EGR level increases from 0 to about 16% EGR. This is a direct consequence of the decrease in the combustion gas temperatures (Figure 13). But, as discussed earlier, as the EGR level increases, it brings the adverse effects of incomplete combustion and the availability destroyed during combustion starts decreasing after about 16% EGR. Further, the availability destroyed during the combustion process is higher for the cooled EGR configuration since this configuration results in lower combustion gas temperatures than for the adiabatic EGR configuration.

For the adiabatic EGR configuration (Figure 15), the results are a little less straight forward. This is due to the combined effects (as EGR increases) of increasing inlet temperatures (causing higher combustion temperatures and heat transfer rates), and of increasing dilution (causing lower combustion temperatures and heat transfer rates). Due to the inlet mixture temperature trends with increasing EGR (Figure 9), the importance of these effects changes as EGR increases.

For the adiabatic EGR configuration (Figure 15), the availability associated with the indicated work increases slightly as the EGR increases from 0 to 16% and above 16%

EGR, it starts decreasing. Again, this is the result of the increasing indicated efficiency from 0 to 16% EGR and then decreasing efficiency for higher EGR levels (Figure 11). The net availability leaving with the exhaust flow decreases as EGR increases, and this is a consequence of the decreasing exhaust temperatures as EGR increases.

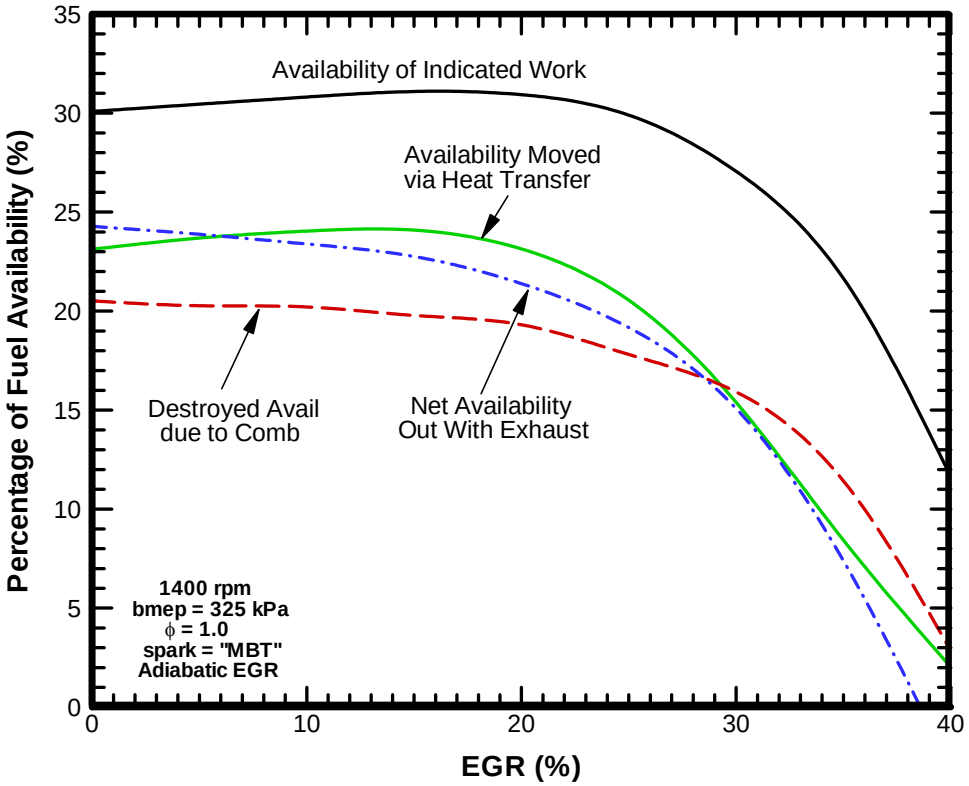

Fig. 15 Four availability terms as functions of the percentage of EGR for the base case conditions for the adiabatic EGR configuration

For the adiabatic EGR configuration for EGR levels greater than about 16%, the availability moved to the cylinder walls via the heat transfer decreases as the percentage of EGR increases. This is due to the lower gas temperatures as the percentage of EGR increases which decreases the temperature difference and hence decreases the heat transfer rates. The adiabatic EGR configuration results in more availability moved to the

cylinder walls than the cooled EGR configuration since the adiabatic EGR configuration results in the higher gas temperatures.

For the adiabatic EGR configuration for EGR levels less than about 16%, the availability moved to the cylinder walls increases as the percentage of EGR increases. For this configuration (adiabatic) and this range of EGR levels, the average combustion gas temperature is essentially constant (Figure 12). The increase of the availability moved to the cylinder walls is due to the increase in the heat transfer coefficient [**25**] due to the increase of the cylinder pressure and the associated changes in the thermodynamic properties as EGR levels increase. This increase of the heat transfer coefficient as EGR levels increase continues for higher levels of EGR (greater than 16%), but the relative importance of the temperature decrease in this range (16% to 40%) dominates over the slight increase of the heat transfer coefficient.

For the adiabatic EGR configuration (Figure 15) for EGR levels between 0% and about 16%, the availability destroyed during the combustion process remains almost constant with increases in the percentage of EGR. For these conditions, the average combustion gas temperature is essentially constant. In addition, the thermodynamics favor work extraction (increasing indicated thermal efficiency, Figure 11). Finally, the heat transfer increases (and the availability moved with the heat transfer increases) for EGR levels between 0% and about 16%. These items combine so that the destruction of availability during the combustion process remains constant for this range of EGR levels.

For the adiabatic EGR configuration for EGR levels greater than about 16%, the availability destroyed during the combustion process decreases very rapidly with further increases in the EGR levels. For this range of EGR, the combined effect of the decrease in the combustion temperature (and the related decrease in the heat transfer) and the decrease in the work extraction (indicated work decreases) causes rapid decrease in availability destroyed during combustion.

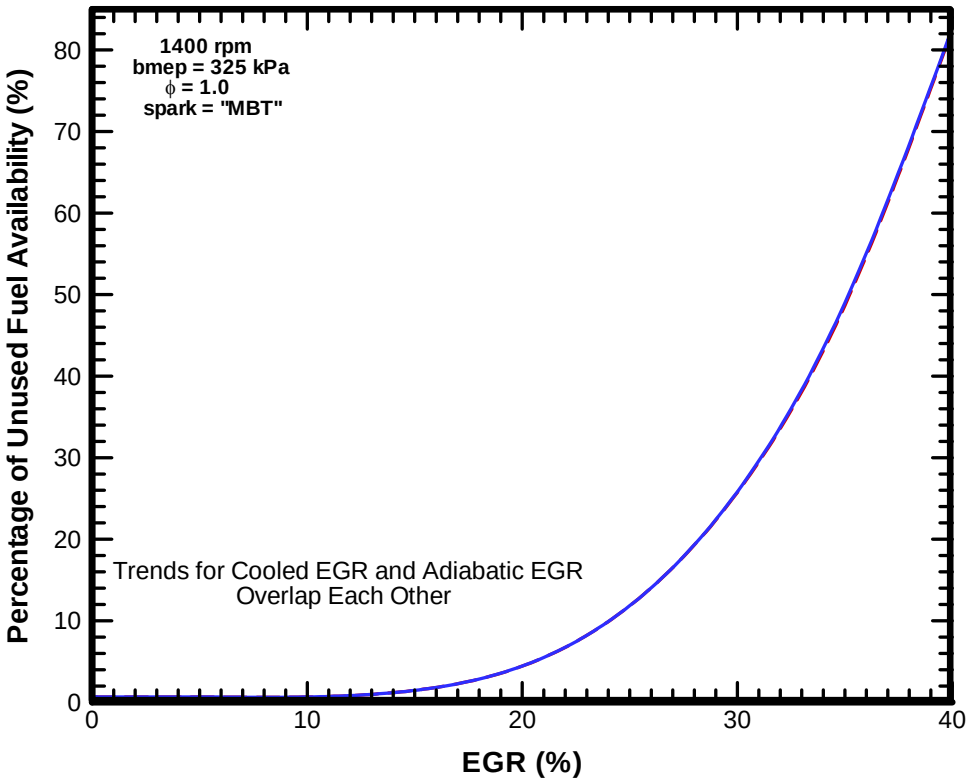

Fig. 16 Percentage of unused fuel availability as functions of percentage of EGR for the base case conditions for both cooled and adiabatic EGR configuration

As shown in Figure 16, the percentage of unused fuel availability remains constant (between 0 and 1%) for EGR levels between 0 and about 12% and then starts increasing rapidly as EGR percentage increases above 12%. This trend is the inverse of the fuel fraction burned schedule. For lower EGR levels, the unburned fuel fraction is not considerable but at higher levels of EGR (above about 12%), the unburned fuel fraction increases from about 1% to 80%. Also, this trend is exactly the same for both cooled and adiabatic EGR configuration.

Returning to Figures 14 and 15, the net availability leaving the cylinder with exhaust is higher for the cooled EGR case since this case has the higher net temperature difference. To understand this trend, Figure 17 shows the difference between the average

exhaust gas temperature and the inlet mixture temperature as the percentage of EGR increases for the two EGR configurations. (For reference, this figure also repeats the plots of the exhaust and inlet mixture temperatures.) This temperature difference decreases as the percentage of EGR increases. Further, the cooled EGR case results in a higher temperature difference than the adiabatic case. This is because for the adiabatic EGR case, the inlet mixture temperature changes (first increases and then rapidly decreases) more (relative to the cooled EGR case) than the exhaust temperature decreases (relative to the cooled EGR case).

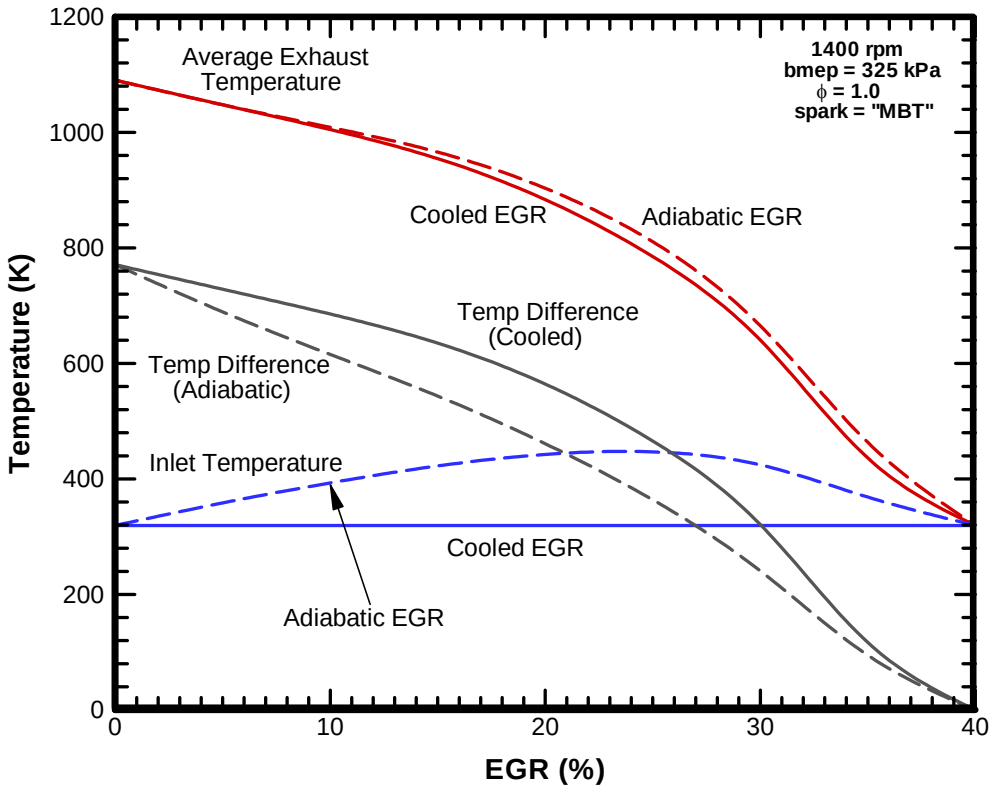

Fig. 17 Average exhaust gas temperatures, inlet mixture temperatures, and the temperature difference (exhaust - inlet) as functions of the percentage of EGR for the base case conditions for both cooled and adiabatic EGR configurations

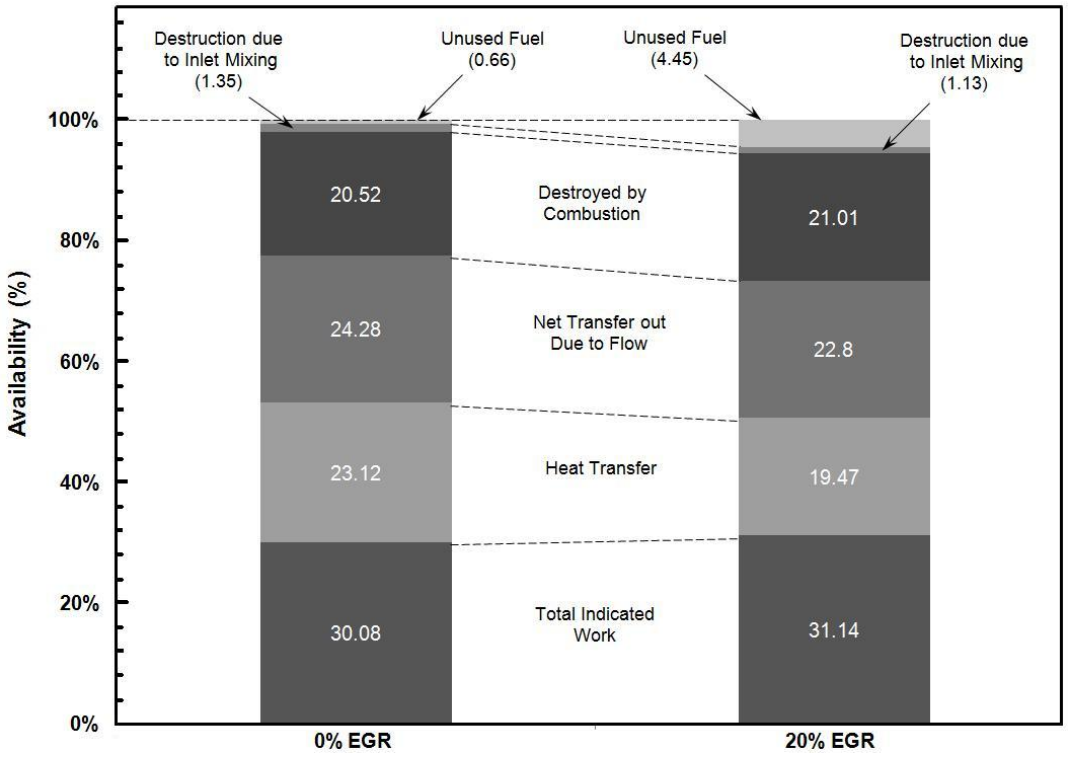

Fig. 18 Percentage of the fuel availability for various items for the base case conditions for 0% and 20% EGR for the cooled EGR case

Figures 18 and 19 are another way to illustrate these results. These figures show the percentage of the fuel availability (which is 100% availability) that is distributed between indicated work, availability moved to the cylinder walls via heat transfer, net availability out in the exhaust, availability destroyed during combustion, availability destroyed by mixing and unused availability (unburned fuel). Figures 18 and 19 show these results for the cooled and adiabatic configurations, respectively, for 0% and 20% EGR. (The 0% EGR case is the same for both configurations.) The major differences between the two configurations are that the adiabatic EGR case, relative to the cooled EGR case, has lower combustion destruction and lower availability in the exhaust, but higher availability moved via heat transfer. As mentioned above, the indicated thermal efficiencies are almost the same for the two EGR configurations.

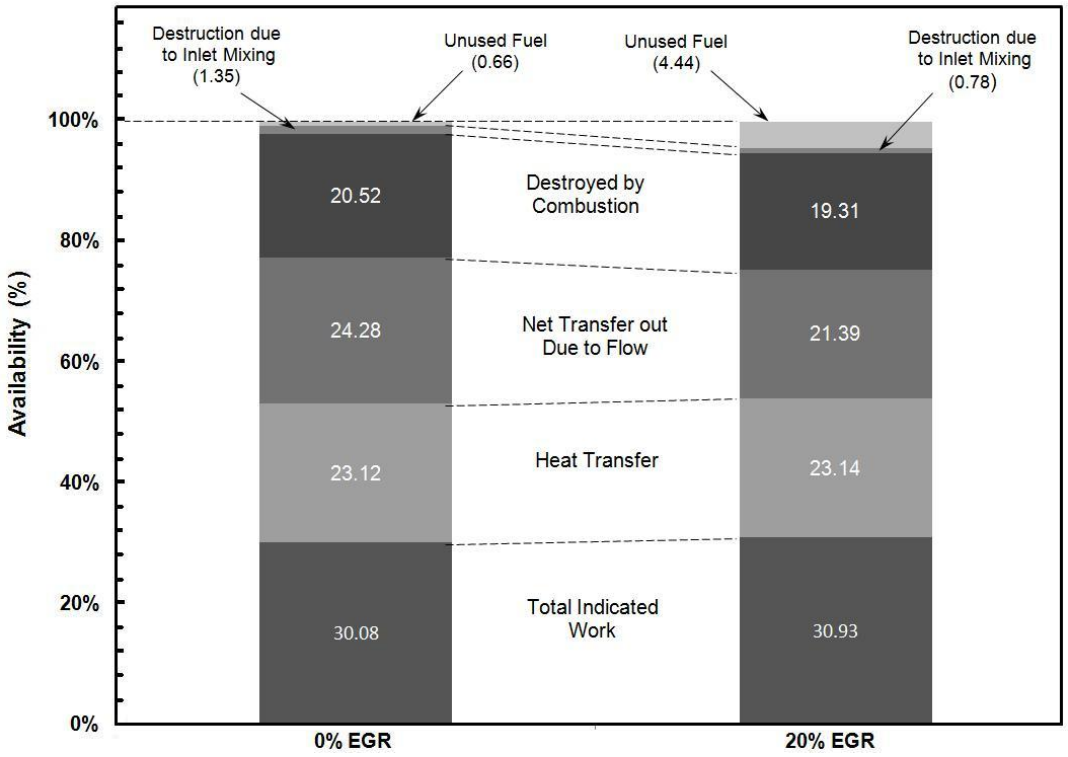

Fig. 19 Percentage of the fuel availability for various items for the base case conditions for 0% and 20% EGR for the adiabatic EGR case

Finally, these results may be used to help explain the results of Figure 11 which showed the thermal efficiencies were similar for both the cooled and adiabatic EGR configurations. For the adiabatic EGR case (relative to the cooled EGR case), the combustion destroyed availability and the net availability that leaves the cylinder with the exhaust gases are less, but the availability moved to the cylinder walls via heat transfer is higher. For the cooled EGR case (relative to the adiabatic EGR case), the availability moved to the cylinder walls via heat transfer is much less, but this is balanced by the higher amounts of availability in the exhaust and destroyed during the combustion process. The net effect, at least for these conditions, is that the thermal efficiencies are about the same for both EGR configurations.

5.6.2 Variable Load and Speed Results

The second part of this study was to determine and evaluate engine performance as functions of engine load and speed for EGR levels of 0% and 20% with fuel fractions 1.0 and 0.955, respectively (for both adiabatic and cooled EGR configurations). Again, the start of combustion was adjusted to maximize brake mean effective pressure for each condition.

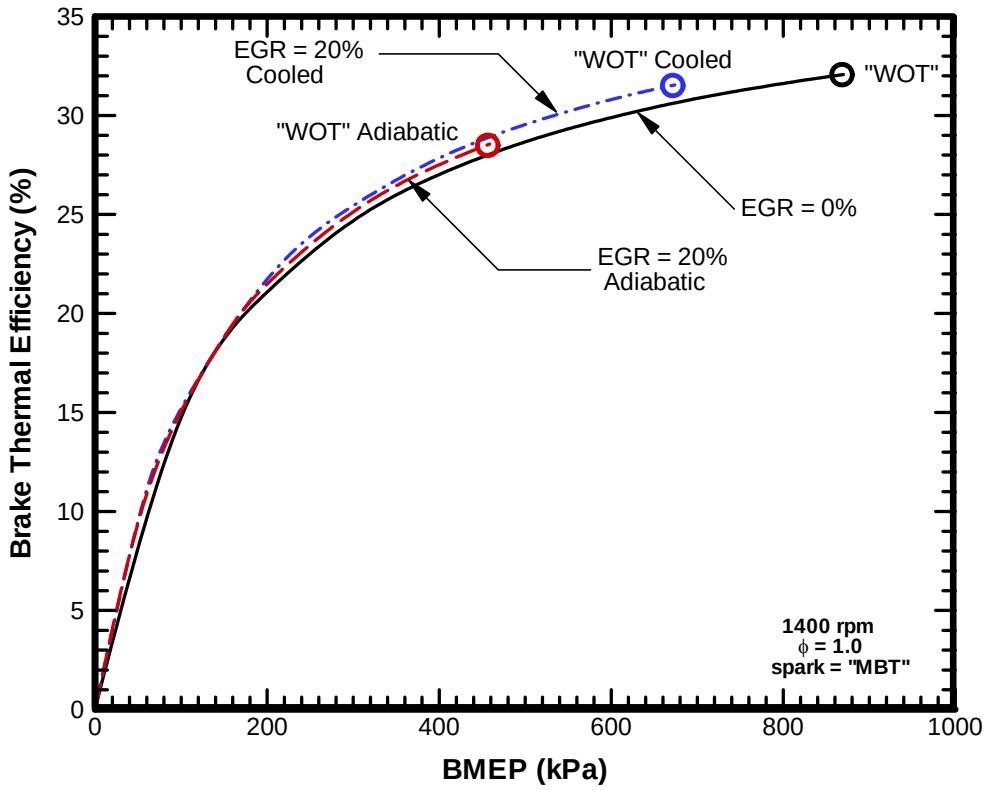

Fig. 20 Brake thermal efficiency as functions of the engine load (bmep) for the base case conditions for 0% EGR and for both cooled and adiabatic EGR configurations with 20% EGR

Results as Functions of Load (bmep)

Figure 20 shows the brake thermal efficiency as functions of engine load (bmep) for the base case with 0% EGR (fuel fraction 1.0) and for the two EGR configurations with 20% EGR (fuel fraction 0.955) for an engine speed of 1400 rpm. The brake efficiency increases with increasing load largely due to the reduction in the throttle losses (*i.e.*, reduction of pmep). Wide open throttle (WOT) was defined as an inlet manifold pressure of 95.0 kPa. For this manifold pressure, a maximum bmep was obtained for each of the three cases. This operating point is shown in Figure 20 with a circle. The maximum bmep for the EGR cases is lower than for no EGR, and is lowest for the adiabatic EGR case. As indicated above, the brake efficiency is higher for the EGR cases, and is approximately of equal magnitude for the two EGR configurations.

Figure 21 shows the relative heat transfer as functions of engine load (bmep) for the three cases for an engine speed of 1400 rpm. Again, the relative heat loss is the percentage of the fuel energy which is transferred to the cylinder walls via heat transfer. The relative heat loss decreases with increasing engine load. Although the heat transfer rates increase with increasing engine load, the fuel energy input increases more rapidly with increasing load. The net effect is that the relative heat loss (the ratio of actual heat transfer energy and fuel input energy) decreases as engine load increases. The relative heat transfer decrease is most significant as bmep increases from no load to about 300 kPa. For engine loads (bmep) greater than about 300 kPa, the decrease of the relative heat transfer is much less rapid as a function of load.

The actual heat transfer is lower for both EGR configurations due to the lower gas temperatures. The comparisons based on the relative heat transfer, however, are different. Below 120 kPa bmep, the base case with 0% EGR has slightly higher relative heat transfer than that with the adiabatic EGR configuration. But the adiabatic EGR configuration has higher relative heat transfer compared to 0% EGR case above 120 kPa bmep. At a given engine load, the adiabatic EGR configuration has relatively lower combustion temperature, and higher cylinder pressure than non-EGR case. It is already stated in the earlier foot note that heat transfer coefficient increases as cylinder pressure

increases. At bmeps lower than 120 kPa, the effect of lower combustion temperatures is more significant than the effect of higher heat transfer coefficient. But at the loads above 120 kPa, cylinder pressures are much higher for adiabatic EGR configuration, which causes heat transfer coefficients to be much higher than that of non-EGR case and the effects of heat transfer coefficient gain more significance over the effects of lower combustion temperatures. Hence the trends of relative heat transfer change as shown in Figure 21. The cooled EGR configuration with 20% EGR has the lowest relative heat transfer as the effects of lower gas temperature is always significant.

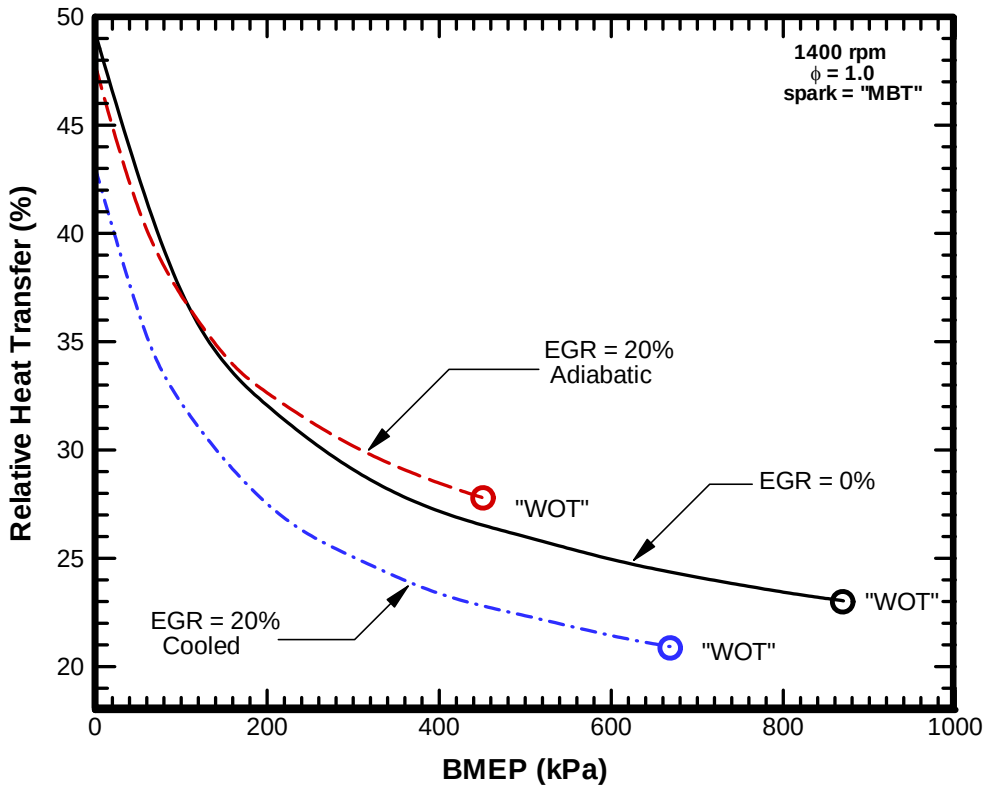

Fig. 21 Relative heat loss as functions of brake mean effective pressure for the base case conditions for 0% EGR and for both cooled and adiabatic EGR configurations with 20% EGR

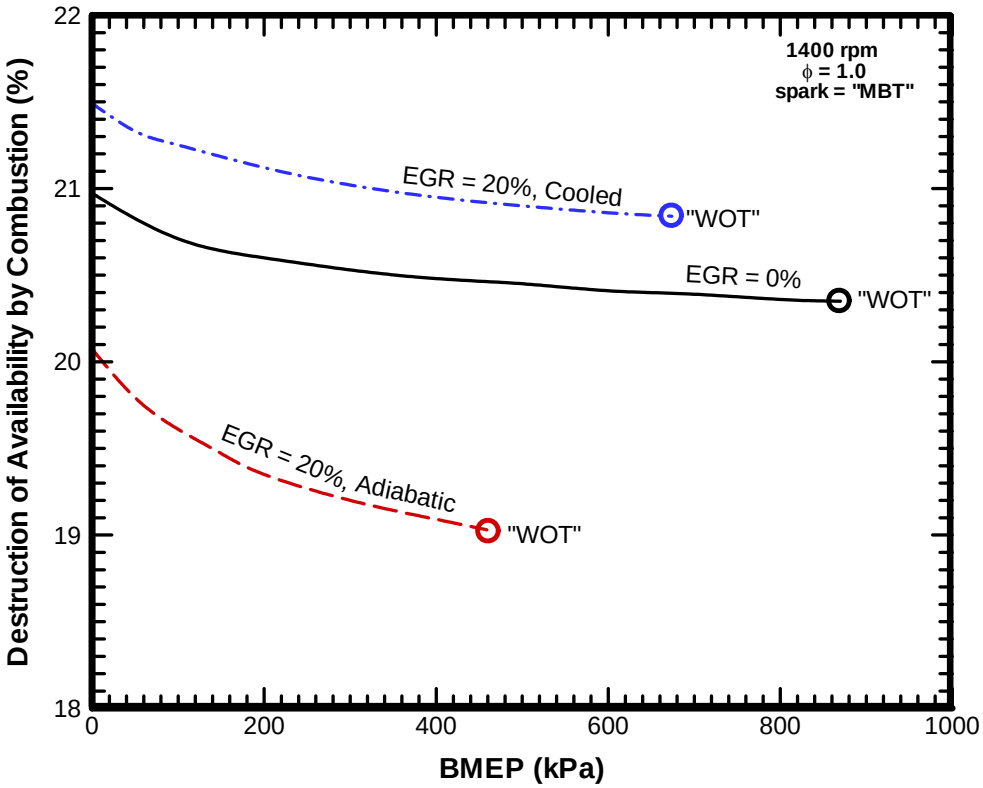

Fig. 22 Percentage of fuel availability destroyed during the combustion process as functions of brake mean effective pressure for the base case conditions for 0% EGR and for both cooled and adiabatic EGR configurations with 20% EGR

Figure 22 shows the percentage of the fuel availability destroyed during the combustion process as functions of engine load (bmep) for the base case with 0% EGR and for the two EGR configurations with 20% EGR. The destroyed availability ranges from about 19.1% to 21.5% for these conditions. The destroyed availability decreases as engine load increases due to the higher combustion temperatures for the higher loads. The destroyed availability is highest for the cooled EGR configuration (lowest combustion temperatures). The 20% adiabatic EGR configuration results in lowest destruction of availability during combustion process because of the higher combustion temperatures relative to the cooled EGR configuration and larger fraction of unburned

fuel relative to 0% EGR case. The non-EGR configuration results in destroyed availability between the other two configurations.

Results as Functions of Speed

Figure 23 shows the brake thermal efficiency as functions of engine speed for a constant engine load (bmep = 325 kPa) for the three cases. For the adiabatic configuration with 20% EGR, even for the lowest speeds, the inlet manifold pressure was already near WOT (81.5 kPa). For this reason, the range of operation was not as large as 0% EGR and 20% cooled EGR case.

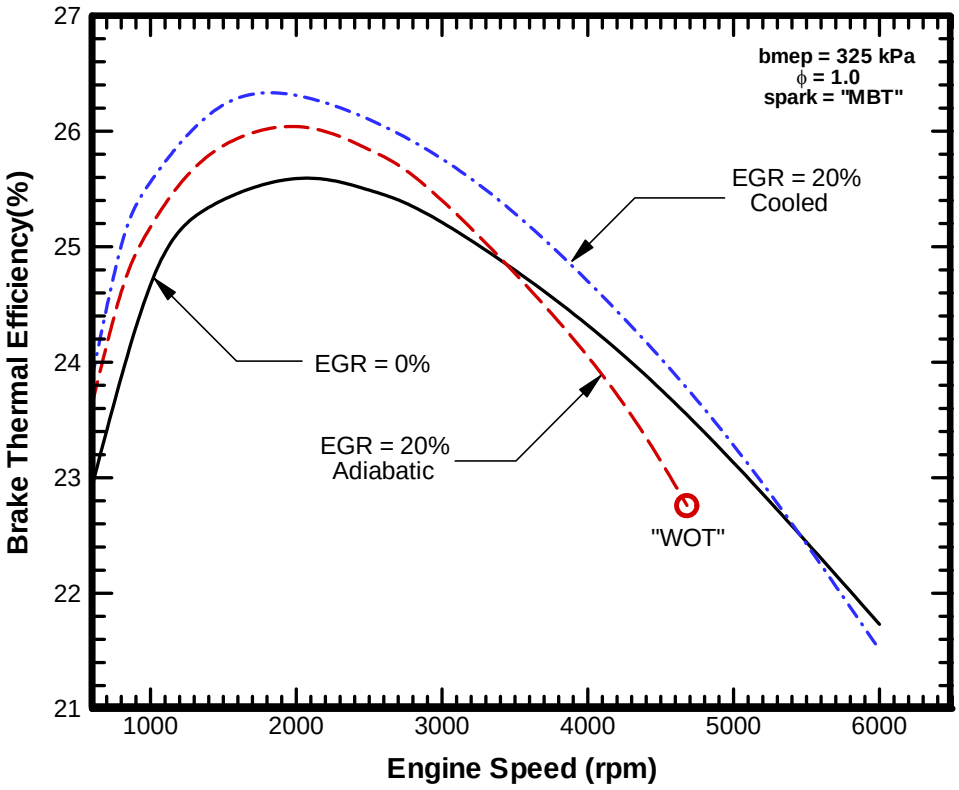

Fig. 23 Brake thermal efficiency as functions of the engine speed for the base case conditions for 0% EGR and for both cooled and adiabatic EGR configurations with 20% EGR

For all three cases, the brake efficiency first increases, reaches a maximum (for engine speeds between about 1600 and 2000 rpm), and then decreases as engine speed increases. The efficiency first increases as engine speed increases due to the importance of decreasing relative heat losses (see discussion below with Figure 25). As engine speed increases, increases in the mechanical frictional losses become more significant than the gains from reduced relative heat transfer, and the brake efficiency decreases. For 20% adiabatic case above about 3500 rpm, relative heat transfer is considerably higher than the non-EGR case due to increased heat transfer coefficient (because of higher cylinder pressure) and it results in lower efficiency for 20% adiabatic than that for 0% EGR.

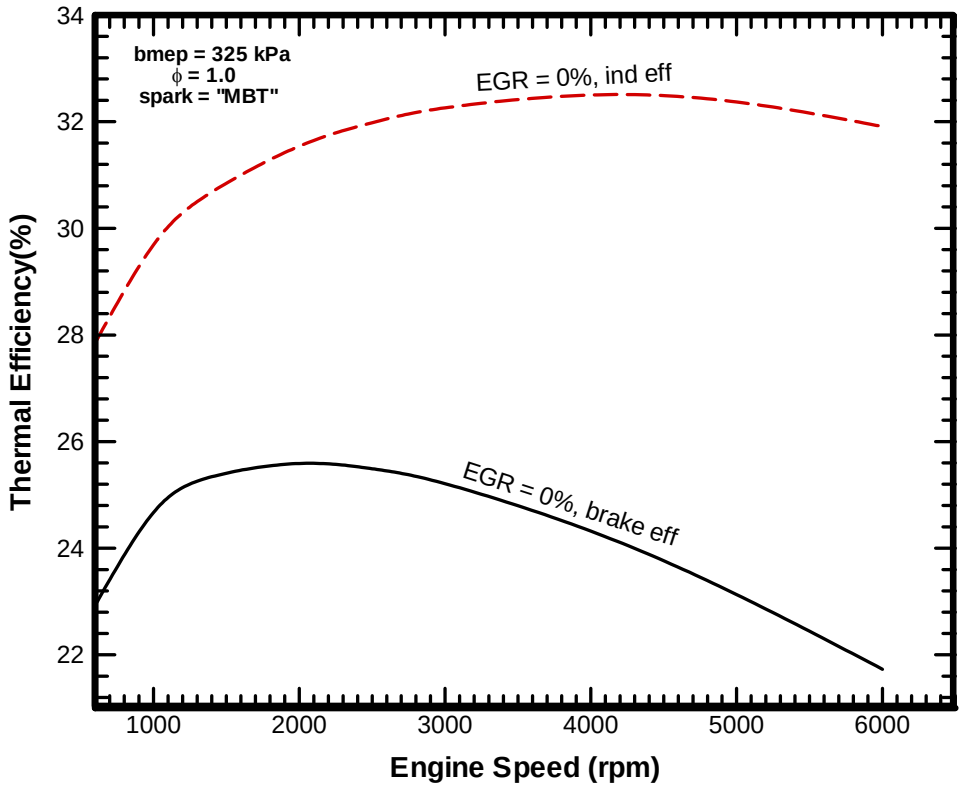

Fig. 24 Indicated and brake thermal efficiencies as functions of the engine speed for the base case conditions for 0% EGR

To complete the discussion of efficiencies, Figure 24 shows the indicated and brake thermal efficiencies as functions of engine speed for the 0% EGR case. The indicated efficiency increases as engine speed increases until about 4200 rpm, and then begins to decrease slightly. This slight decrease is due to the changes in the thermodynamic properties as temperatures increase at higher speed. The brake thermal efficiency increases up to about 2000 rpm for these conditions due to the reduced importance of the relative heat losses. For engine speeds above about 2000 rpm, the brake thermal efficiency decreases due to the more rapidly increasing frictional losses.

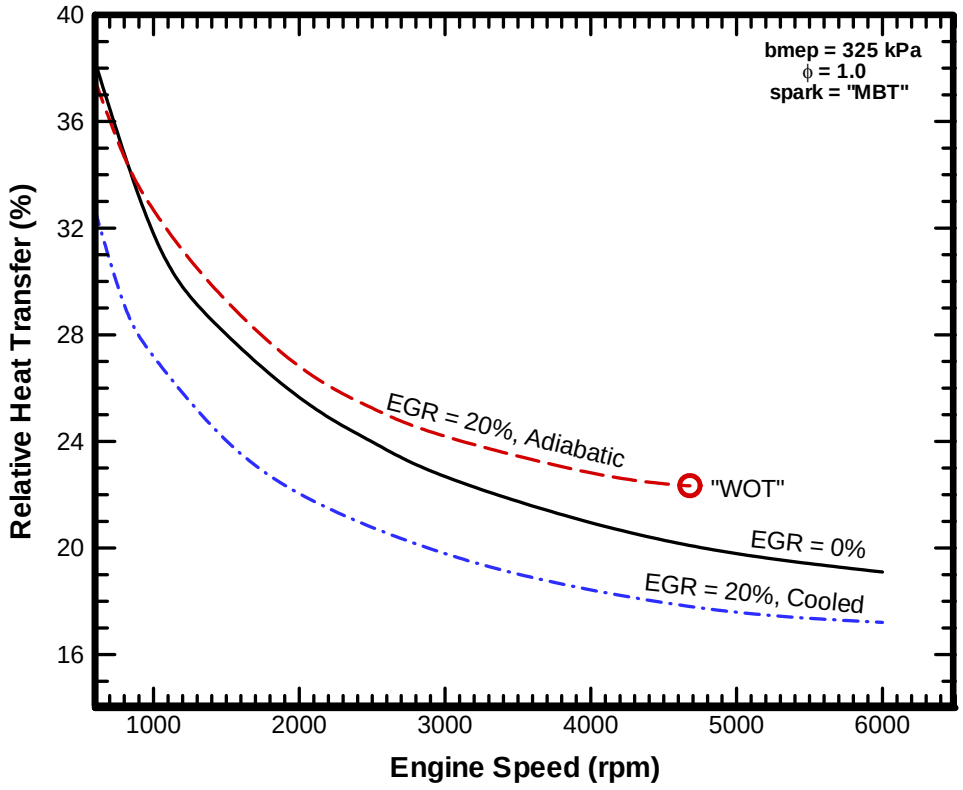

Fig. 25 Relative heat loss as functions of engine speed for the base case conditions for 0% EGR and for both cooled and adiabatic EGR configurations with 20% EGR

Figure 25 shows the relative heat loss as functions of the engine speed for the base case, for the 0% EGR case and for the two EGR configurations with 20% EGR. As mentioned above, the relative heat loss is the percentage of the fuel energy which is transferred to the cylinder walls via heat transfer. The relative heat loss decreases with increasing engine speed. Although the heat transfer rates increase slightly with increasing engine speed, the time available for energy transfer decreases more rapidly. The net effect is that the relative heat loss decreases as engine speed increases. The greatest effect is for the engine speed increase from 600 rpm to about 3500 rpm. For engine speed increases above about 3500 rpm, the decreases in the relative heat loss is much more modest. These effects are consistent for all three cases.

The relative heat transfer (Figure 25) is lowest for the cooled EGR configuration due to the lower temperatures. For engine speeds greater than about 800 rpm, the relative heat transfer is higher for the adiabatic EGR configuration than that for the non-EGR configuration; and it is considerably higher above engine speeds of 3500 rpm which results in the thermal efficiency for adiabatic configuration to be less than that for non-EGR configuration at the engine speeds above 3500 rpm.

Figure 26 shows the percentage of the fuel availability that is destroyed during the combustion process as functions of engine speed for the base case conditions with 0% EGR, and for the two EGR configurations with 20% EGR. The percentage attributed to the combustion destroyed availability for these conditions ranged from about 18.2% to 21.7%. The combustion destroyed availability decreases with engine speed (due to the higher temperatures), and is highest for the cooled EGR configuration using 20% EGR (lowest combustion temperatures, Figure 12). The adiabatic EGR configuration results in the lowest combustion destroyed availability because of combine effect of higher combustion temperatures and unused fuel fraction. And the non-EGR configuration is between the other two configurations.

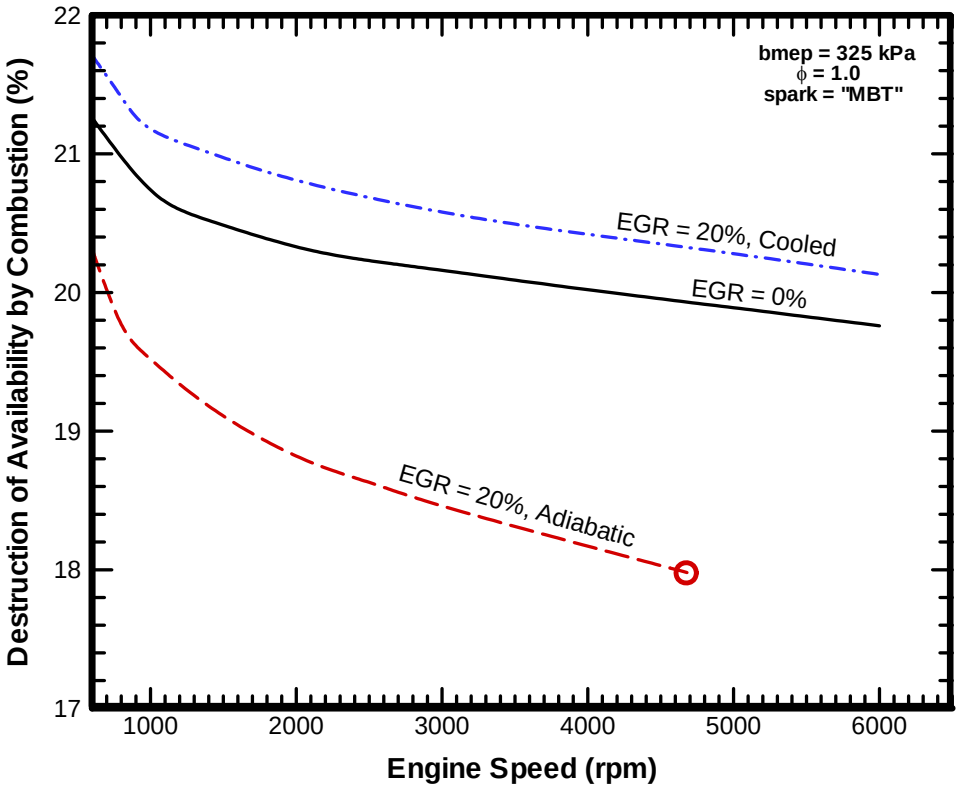

Fig. 26 Percentage of fuel availability destroyed during the combustion process as functions of engine speed for the base case conditions for 0% EGR and for both cooled and adiabatic EGR configurations with 20% EGR

6. SUMMARY, CONCLUSIONS, AND RECOMMENDATIONS

A thermodynamic cycle simulation of a four stroke spark-ignition engine was used to examine the use of exhaust gas recirculation for a spark ignition engine from both a first law and second law perspective. Combustion instability effects at higher EGR levels were considered. A parameter called Fuel Fraction Burned was introduced in the model to include the combustion instability effects. Two EGR configurations, cooled and adiabatic, were examined. In the first part of the study, a complete set of results were obtained for a fixed engine load (bmep=325 kPa) and engine speed (1400 rpm). The efficiency results were compared with the available experimental data and a good correlation was obtained between the simulated and the experimental trends of efficiency. In the second part of the study, general results were obtained as functions of engine load and speed.

The results of the parametric study may be summarized as follows:

1. For both EGR configurations, the level of nitric oxide emissions reduces with increases in EGR levels. However, for the same EGR level, the cooled EGR configuration results in the greatest nitric oxide reductions. Even though the model is not capable of calculating the hydrocarbon emissions, it can be predicted from the unused fuel availability values that at higher levels of EGR hydrocarbon emissions would be expected to be high.
2. Both EGR configurations result in approximately the same brake and indicated thermal efficiencies. At the same load, the heat losses are less for the cooled EGR configuration and the pumping losses are less for the adiabatic EGR configuration. At any given EGR level, these two effects are of approximately equal magnitude and hence the efficiencies are approximately same. For both configurations, first the efficiencies increase and then decrease as the EGR level increases. Above 25% EGR, the drops in the efficiencies are very fast with increasing EGR and it is the consequence of higher combustion instabilities at higher EGR levels.

3. At lower EGR levels, the availability destroyed during the combustion process increases for cooled EGR configuration and it is constant for adiabatic EGR configuration. But both configurations result in steep reduction in the availability destroyed during the combustion process at higher EGR levels. At higher EGR levels, very high frequency of the occurrence of combustion patterns like partial burn and misfire result in large fraction of the fuel to be remained unburned and availability destroyed in the combustion to reduce. However, at a given EGR level, the cooled EGR configuration results in greater availability destroyed during combustion.
4. Relative heat losses decrease as the EGR level increases. This is a direct consequence of decreasing gas temperature inside the cylinder as the EGR rate increases. However relative heat transfer increases slightly at lower EGR levels for adiabatic EGR configuration, it decreases rapidly at higher levels of EGR. The adiabatic EGR configuration results in greater relative heat transfer than the cooled EGR configuration.
5. The brake thermal efficiencies increase as engine load increases and these increments are largely due to increased P_{in} with increasing load because as P_{in} increases it imposes less throttle restriction. The brake thermal efficiency is slightly higher for EGR cases and approximately of equal magnitude for both EGR configurations. The EGR cases are limited to lower maximum engine load at wide open throttle (WOT).
6. The relative heat losses decrease with increasing engine load, and the cooled EGR configuration results in the lowest relative heat losses. The adiabatic EGR configuration and non-EGR configuration have about equal relative heat losses.
7. The availability destroyed during the combustion process decreases as the engine load increases largely due to the increase in gas temperatures for both EGR configurations. However, the cooled EGR configuration results in the highest destruction of availability due to combustion, and the adiabatic EGR configuration results in the lowest.

8. The brake thermal efficiencies first increase, and then decrease as the engine speed increases. At lower engine speeds, the importance of decreasing relative heat losses with increasing speeds causes the increase in the efficiency. At higher engine speeds, friction losses are very significant, and more important, which causes decreases in thermal efficiencies. At lower and medium engine speeds, cooled EGR configuration results in the highest efficiency, and both EGR configurations have higher efficiency than non-EGR configuration, but at very high speeds non-EGR case results in the highest efficiency.
9. The relative heat losses decrease as the engine speed increases and it is the minimum for the cooled EGR configuration. The heat transfer rate increases with engine speed but time available for the heat transfer decreases more rapidly.
10. The destruction of availability due to combustion decreases as the engine speed increases due primary to resulting higher temperatures as the relative heat losses decrease.

As described above, the computed NOx emission characteristics, with the use of EGR, are similar to the results of previous experimental and computational studies. At the higher EGR levels, the results of engine performance parameters deviate from the results of some previous computational study. This is primarily due to the reason that the previous study does not consider the combustion instability issues which are significant at the higher EGR levels. The maximum thermal efficiencies are resulted in the previously suggested range of optimal EGR levels (between 15% and 20% EGR) for both EGR configurations. The variable load and speed results are also in close approximation with the previous computational studies.

One of the main conclusions from this study is that EGR (between about 10% and 20%) can be used to reduce nitric oxide emissions as well as to improve engine performance (increased thermal efficiencies) over a wide range of operating conditions.

The recommendations for the future work are stated below:

1. Previous experimental studies stated that as EGR levels increase, the frequency of occurrence of different combustion patterns (slow burn, partial burn and misfire, which causes unstable engine operation) increases. Therefore, future thermodynamic model study should consider each of the combustion patterns in specific to determine the engine performance.
2. Engine instability caused by slow burn cycles can be avoided by using short combustion duration (fast burn). Utilization of swirl and squish, and decrease of flame propagation distance are some of the approaches to achieve the fast burn. Although some of the past literatures predicted higher NOx emission with the fast burn [**38, 39**], the potential of the combination of the fast burn and heavy EGR should be studied using thermodynamic cycle simulation.
3. As already stated in one of the assumptions that this study did not consider cycle-by-cycle variation, future studies can be made more realistic by considering cycle-by-cycle variations. However it is very difficult to model thermodynamic cycle simulation which can include such effects as it can be caught through experimental studies only.
4. From the emissions perspectives, the current study was only focused on nitric oxide emissions. The future work should be model to predict hydrocarbon emissions and CO emissions (as they are also regulated species of engine emissions).

REFERENCES

1. **Griffin, R. D.** *Principles of Air Quality Management,* 2nd Edition, 2007 (CRC Press - Taylor & Francis, Boca Raton, FL).

2. **Paul Ih-Fei Liu** *Energy, Technology and the Environment,* 1st Edition, 2005 (ASME Press, New York, NY).

3. **MA, T. H.** Effect of cylinder charge motion on combustion. In Conference on *Combustion in Engines*, Automobile Division of IMechE, Cranfield Institute of Technology, 7-9 July 1975, pp. 1-11.

4. **Mattavi, J. N.** Effects of combustion chamber design on combustion in spark ignition engines. SAE paper 821578, 1982.

5. **Berger, L. B., Elliot, M. A., Holts, T. C., Schrenk, H. H.** Diesel engines underground – II. Effect of adding exhaust gas to intake air. U. S. Department of Interior, Bureau of Mines, R. I. 3541, pp. 7867, November 1940.

6. **Miller, A. E., and Sullis, S.** Recycling exhaust gas for suppressing of knock in ICE. In Proceedings of American Petroleum Institute, Section 111, 1953, pp. 151.

7. **Kopa, R. D., and Kimura, H.** Exhaust gas recirculation as a method of nitrogen oxides control in an internal combustion engine. APCA 53rd Annual Meeting, Cincinnati, OH, May 1960.

8. **Kopa, R. D., Jewell, R., and Spangler, R. V.** Effect of exhaust gas recirculation on automotive ring wear. SAE paper S321, Society of Automotive Engineers, Southern California Section, Los Angeles, CA, 1962.

9. **Musser, G. S., Wilson, J. A., Hyland, R. G., and Ashby, H. A.** Effectiveness of exhaust gas recirculation with extended use. Technical Report PR 64–15, Ford Motor Co., 1964.

10. **Kuroda, H., Nakajima, Y., Sugihara, K., Takagi, Y., Muranaka, S.** The fast burn with heavy EGR, new approach for low NOx and improved fuel economy. SAE paper 780006, *SAE Trans.*, 1978, **87**, 5-7.

11. **Cha, J., Kwon, J., Cho, Y., Park, S.** The effect of exhaust gas recirculation (EGR) on combustion stability, engine performance and exhaust emissions in a gasoline engine. *KSME International Journal,* 2001, **15**, 1442-1450.

12. **Gardiner, D. P., Bardon, M. F., Rao, V. K.** Effects of prompt EGR on warm-up and steady state fuel consumption and emissions. SAE paper 912374, 1991.

13. **Lebel-Simon, M., Cottereau, M. J.** Simultaneous cars measurements of temperature of CO_2 concentration applied to the study of the effect of the residual gas fraction on combustion in an SI engine. In Proceedings of the Third International Symposium on *Modelling and Diagnostics in Internal Combustion Engines* (*COMODIA 94*), 1994, pp. 465–470.

14. **Martin, J. K., Plee, S. L., Remboski Jr, D. J.** Burn modes and prior-cycle effects on cyclic variations in lean-burn spark-ignition engine combustion. SAE paper 880201, 1988.

15. **Belmont, M. R., Hancock, M. S. and Buckingham, D. J.** Statistical aspects of cyclic variability. SAE paper 860324, 1986.

16. **Quader, A. A.** What limits lean operation in spark ignition engines – flame initiation or propagation? SAE Paper 760760, *SAE Trans.*, 1976, **85**.

17. **Deeter, W. F., Daigh, H. D., and Wallin, O. W., Jr.** An approach for controlling vehicle emissions. SAE paper 680400, 1968.

18. **Jacobs T., Assanis D., Filipi Z.** The impact of exhaust gas recirculation on performance and emissions of a heavy-duty diesel engine. SAE Paper 2003-01-1068, 2003.

19. **Ladommatos, N., Abdelhalim, S., Zhao, H. and Hu, Z.** The effects of carbon dioxide in exhaust gas recirculation on diesel engine emissions. *Proc. IMechE, Part D, Journal of Automobile Engineering,* 1998, **212**, 25–42.

20. **Newhall, H. K.** Control of nitrogen oxides by exhaust recirculation – a preliminary theoretical study. SAE paper 670495, 1967.

21. **Caton J. A.** Utilizing a cycle simulation to examine the use of EGR for a spark-ignition engine including the second law of thermodynamics. In 2006-Fall conference of the ASME Internal Combustion Engine Division, ICEF 2006-1508.

22. **Aleiferis, P. G., Taylor1, A. M. K. P., Ishii, K., Urata, Y.** The relative effects of fuel concentration, residual-gas fraction, gas motion, spark energy and heat losses to the electrodes on flame-kernel development in a lean-burn spark ignition engine. *Proc. IMechE, Part D, Journal of Automobile Engineering,* 2004, **218**, 411-425.

23. **Patterson, D. J. and Van Wylen, G. J.** A digital computer simulation for spark-ignited engine cycles. SAE *Progress in Technology* Series, SAE Inc, New York, 1964, **7**, 88.

24. **Caton, J. A.** A review of investigations using the second-law of thermodynamics to study internal- combustion engines. In *SI Combustion*, SP–1517, SAE paper 2000–01–1081, pp. 9–22, at the 2000 SAE International Congress and Exposition, Cobo Center, Detroit.

25. **Caton, J. A.** The effects of exhaust gas recirculation (EGR) on engine performance, available energy and nitric oxide emissions for a spark-ignition engine: results from a thermodynamic cycle simulation. Report No. ERL–2006–01, Engine Research Laboratory, Department of Mechanical Engineering, Texas A&M University, 24 March 2006.

26. **Caton, J. A.** A multiple-zone cycle simulation for spark-ignition engines: thermodynamic details. In *Large-Bore Engines, Fuel Effects, Homogeneous Charge Compression Ignition, Engine Performance and Simulation, Vol. 2, ICE-Vol. 37–2,* Proceedings of the 2001-Fall Technical Conference, ed. V. W. Wong, the ASME `Internal Combustion Engine Division, ASME paper 2001–ICE–412, pp. 41– 58, Argonne, IL, 23–26 September 2001.

27. **Woschni, G.** A universally applicable equation for the instantaneous heat transfer coefficient in the internal combustion engine. SAE paper 670931, *SAE Trans.*, 1968, **76**, 3065–3083.

28. **Wiebe, J. J.** Brennverlauf und Kreisprozess von Verbrennungsmotoren. VEB-Verlag Technik Berlin, 1970.

29. **Heywood, J. B.** *Internal Combustion Engine Fundamentals*, 1988 (McGraw-Hill Book Company, New York, NY).

30. **Heywood, J. B., Higgins, J. M., and Watts, P. A., and Tabaczynski, R. J.** Development and use of a cycle simulation to predict SI engine efficiency and NOx emissions. SAE paper 790291, 1979.

31. **Olikara, C., and Borman, G. L.** A computer program for calculating properties of equilibrium combustion products with some applications to I. C. engines. SAE paper 750468, 1975.

32. **Sandoval, D. and Heywood, J. B.** An improved friction model for spark-ignition engines. SAE paper 2003–01–0725, 2003.

33. **Dean, A. M. and Bozzelli, J. W.** Combustion chemistry of nitrogen. In *Gas-Phase Combustion Chemistry*, ed. W. C. Gardiner, Jr., pp. 125–342, Springer-Verlag, New York, 2000.

34. **Caton, J. A.** Detailed results for nitric oxide emissions as determined from a multiple-zone cycle simulation for a spark-ignition engine. In *Design, Application, Performance and Emissions of Modern Internal Combustion Engine Systems and Components, ICE-Vol. 39*, Proceedings of the 2002-Fall Technical Conference, ed. V. W. Wong, the ASME Internal Combustion Engine Division, ASME paper ICEF–2002–491, pp. 131–148, New Orleans, LA, 08–11 September 2002.

35. **Caton, J. A.** The use of a three-zone combustion model to determine nitric oxide emissions from a homogeneous- charge, spark-ignition engine. In Proceedings of the 2003-Spring Technical Conference of the ASME Internal Combustion Engine Division, pp 1-12, Hellbrunn Palace, Salzburg, Austria, 11–14 May 2003.

36. **Caton, J. A.** Effects of compression ratio on nitric oxide emissions for a spark-ignition engine: results from a thermodynamic cycle simulation. *Journal of Engine Research*, 2003, **4**, 249–268.

37. **Caton, J. A.** A cycle simulation including the second law of thermodynamics for a spark-ignition engine: implications of the use of multiple-zones for combustion. SAE paper 2002–01–0007, *SAE Trans. - Journal of Engines,* September 2003, **111–3**, 281–299.

38. **Quader, A. A.** Effects of spark location and combustion duration on nitric oxide and hydro-carbon emissions. SAE paper 730153, 1973.

39. **Hosho, Y., Oyama, Y., Yamauchi, T., Nishimiya, T.** Exhaust emission reduction with lean mixture (2). *Nainen Kikan*, 1974, **13-152,** 11-18.

APPENDIX

Part: 1 Effect of Different Combustion Duration Schedules as Functions of Percentage of Exhaust Gas Recirculation on Thermal Efficiency

As documented earlier, the previous thermodynamic model was extended to incorporate a parameter called Fuel Fraction Burned to consider combustion instabilities. Before a new parameter, FFB (FFB was not an input parameter in the previous model) was introduced in the model and the trials were made to reach to a final FFB schedule, trials were made with an existing parameter, combustion duration ($\Delta\theta_b$). Several combustion duration schedules as functions of EGR percentage were tried. The following paragraph explains why variable combustion duration was chosen for initial trials.

Table 8 Classification of combustion pattern [**10**]

(1400 rpm, $imep_{mean}$= 324 kPa)

Combustion Pattern	**Remark**	**imep (P_i), kPa**	**Crank Angle at Combustion Termination**
Normal Burn	– Short Combustion Duration – Complete Flame Propagation	392> P_i>275	30^o~80^o ATDC
Slow Burn	– Long Combustion Duration – Complete Flame Propagation	275> P_i>147	80^o~EVO
Partial Burn	– Incomplete Flame Propagation	147> P_i>0	Large Variation
Misfire	– Flame not Detected	0> P_i	-

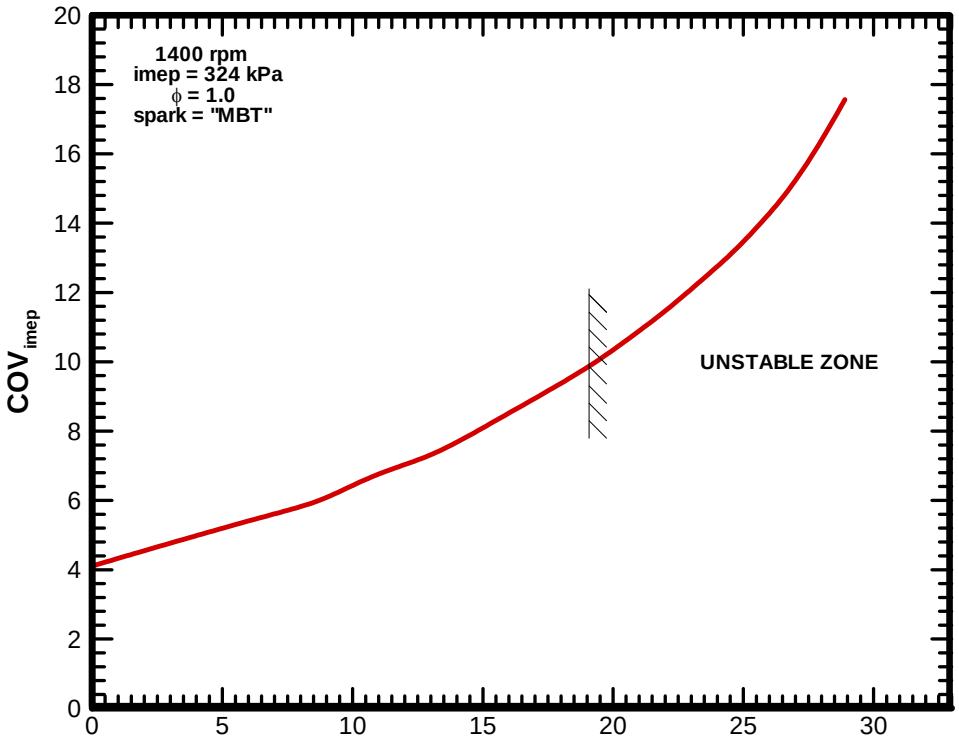

Fig. 27 Effect of EGR on coefficient of variation in imep (COV_{imep}) [**10**], (Redrawn)

Kuroda *et al.* [**10**] collected the combustion period and heat release data from the cylinder pressure traces and compared the data with imep levels. They defined the combustion period as the crank angle where the calculated heat-release stops rising. They observed that the combustion terminates early for the normal burn cycles, while for slow burn cycles combustion is slow and in some cases it lasts until the exhaust valve opens. The imep levels of normal burn cycles were higher than the slow burn cycles (see Table 8) but the calculated heat release was almost same for both patterns.

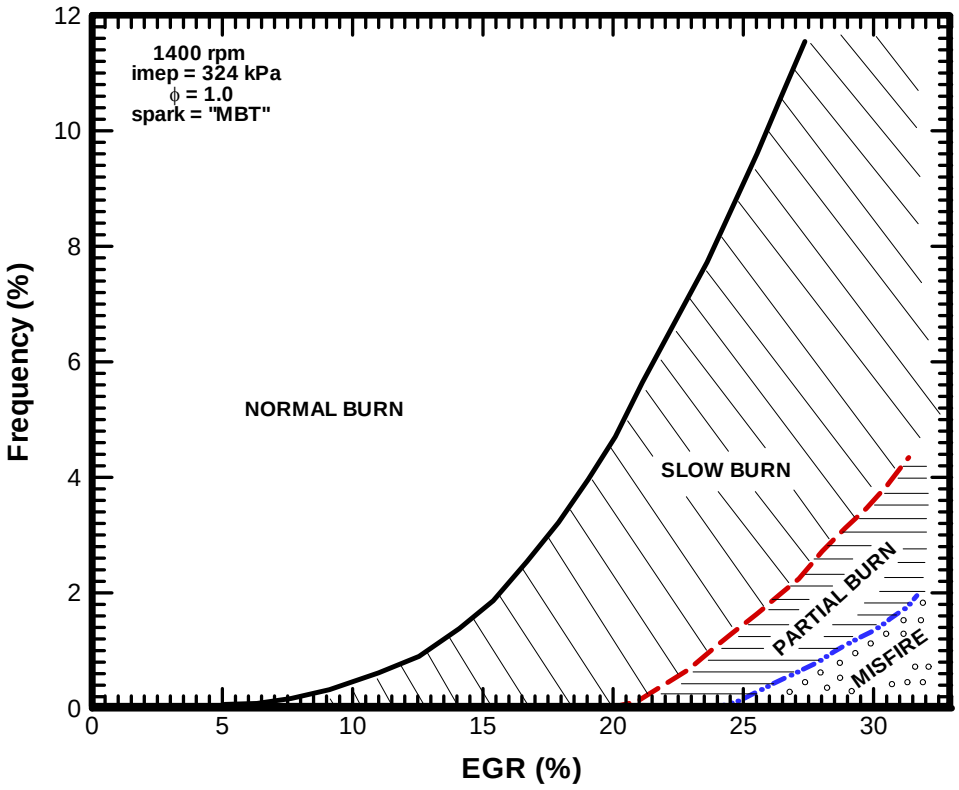

Fig. 28 Effect of EGR on the distribution of combustion patterns [**10**], (Redrawn)

Considering the fact that slow burn cycles have lower imep levels it may be concluded slow burn cycles may be contributing to drop in the thermal efficiencies. Also, out of three combustion patterns which cause unstable engine operation, slow burn cycles appear first at about 8% of EGR and frequency of occurrence reaches to 5% at approximately 20% EGR. The engine reaches the acceptable stability limit at 5% slow burn cycles. The frequency of occurrence of slow burn cycles increases rapidly as EGR levels increase further (see Figure 28).

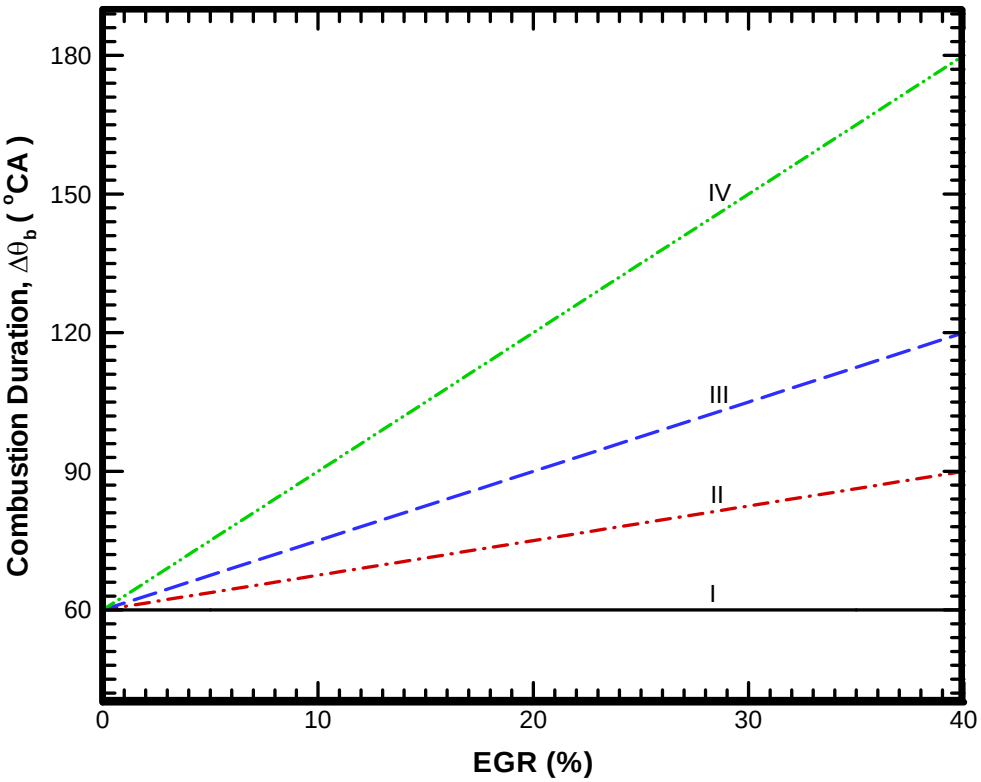

Fig. 29 Four different combustion duration schedules as a function of the percentage of EGR

Considering all these facts four linear combustion duration schedules were tried and efficiency results were compared with experimental results. Figure 29 shows four combustion duration schedules as functions of EGR percentage, and Figures 30 and 31 show the corresponding efficiency trends for each of the schedules for both cooled and adiabatic EGR configuration, respectively.

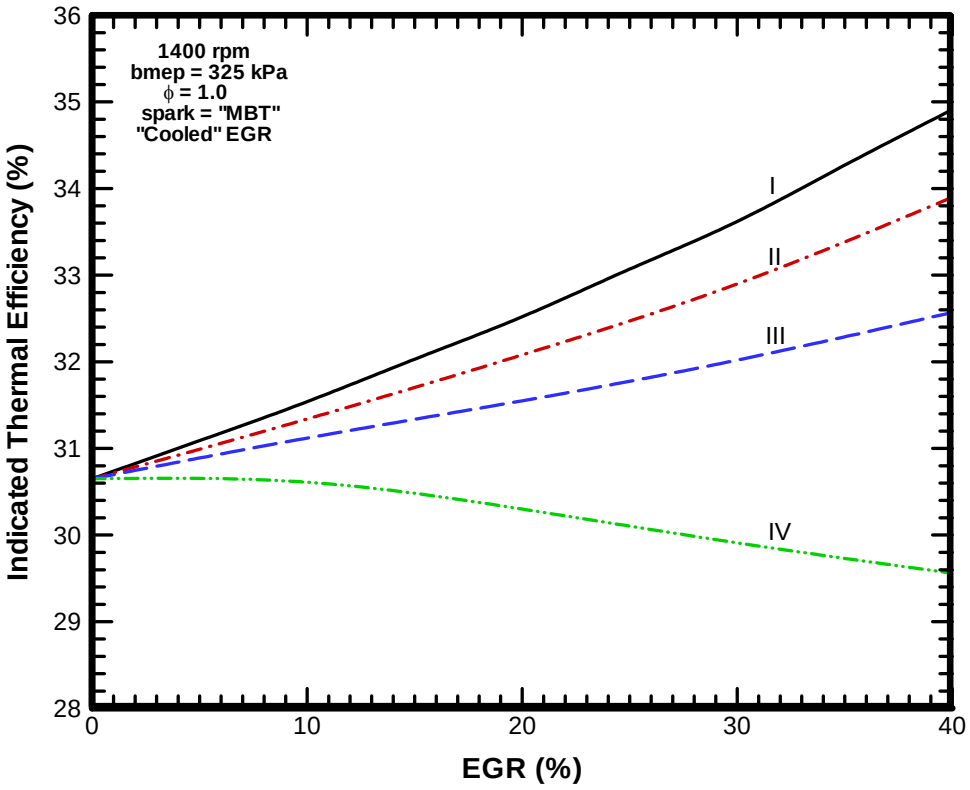

Fig. 30 Indicated thermal efficiency as functions of the percentage of EGR for the four combustion duration schedules for the cooled EGR configuration

The thermal efficiency plots (Figures 30 and 31) show that for schedules I, II, and III the efficiencies increase as the EGR level increases, and the schedule IV shows that the efficiency decreases as the EGR level increases for both EGR configurations. The increasing efficiency trends were totally contradicting with the experimental efficiency trends (see Figure 1). Even the decreasing efficiency trend with the schedule IV did not give close approximation to the efficiency trends from the experimental results.

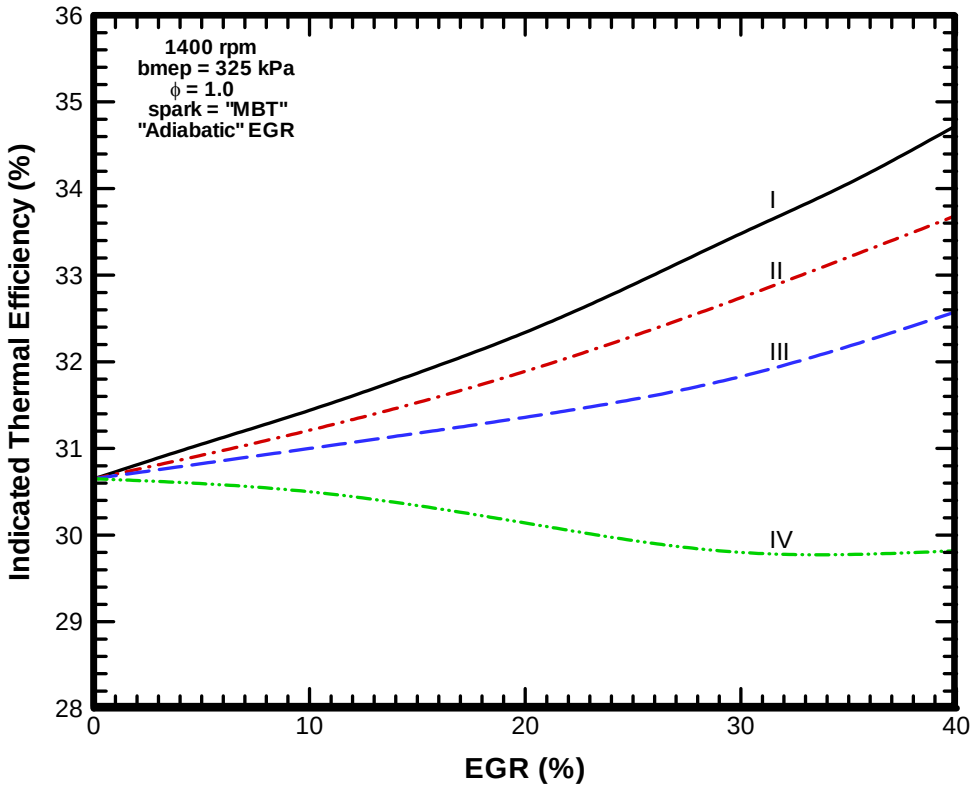

Fig. 31 Indicated thermal efficiency as functions of the percentage of EGR for the four combustion duration schedules for the adiabatic EGR configuration

Part 2: Effect of Different Fuel Fraction Burned Schedules as Functions of Percentage of Exhaust Gas Recirculation on Thermal Efficiency

Different combustion duration schedules were tried, considering the effects of slow burn cycles, but none of the schedules resulted in to an efficiency trend which would be in close approximation to the experimental efficiency trends. Referring to Figure 28, at about 20% EGR, along with several percentages of slow burn cycles partial burn cycles start to appear. Further increase in EGR level results in appearance of misfire cycles along with other two types of combustion pattern.

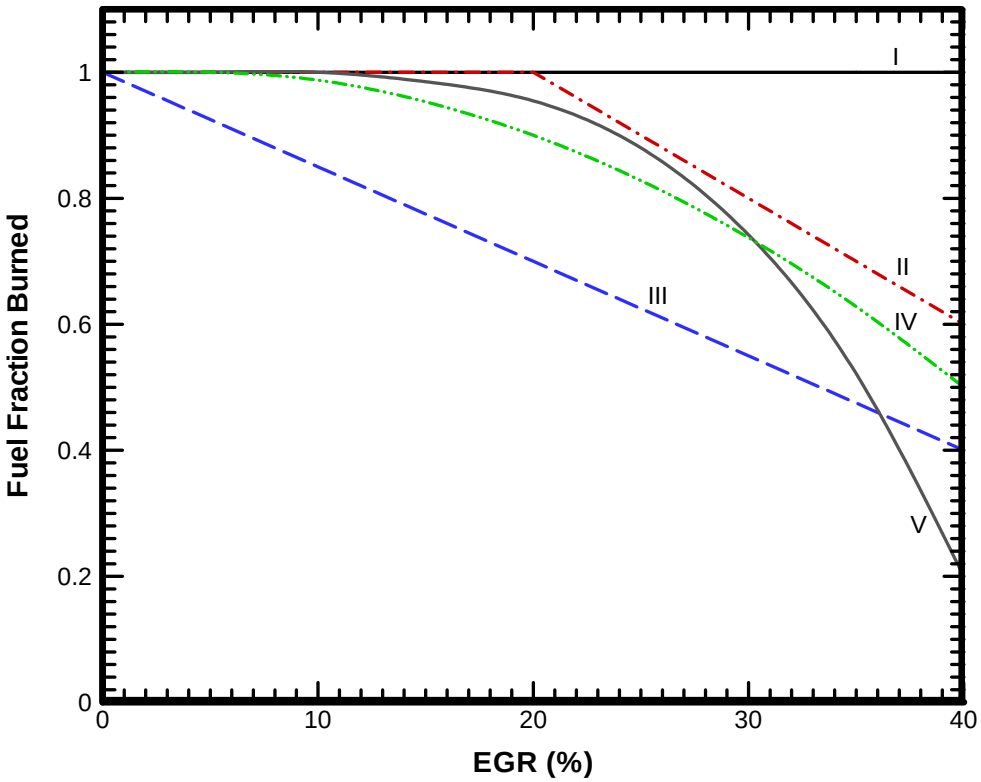

Fig. 32 Five different fuel fraction burned schedules as a function of the percentage of EGR

Table 8 shows classification of combustion pattern and characteristics of all types of combustion pattern. The partial burn cycles are identified as the cycles in which flame propagation is incomplete and 100% of the fuel is not burned. The misfire cycles are the cycles in which combustion does not initiate at all. To catch the effects of partial burn cycles and misfire cycles along with slow burn cycles a new parameter called Fuel Fraction Burned (FFB) was introduced in to the model. As previously defined, FFB is the mass of fuel burned in a cycle to the total mass of fuel entered in the chamber. In short, FFB was selected as the parameter to represent the combined effects of all three types of combustion patterns.

Different FFB schedules, like constant, linear, combination of constant and linear, quadratic, and third order polynomial were tried. Figure 32 shows the five FFB schedules tried as functions of EGR percentage, and Figures 33 and 34 show the corresponding efficiency trends for each of the schedules for both cooled and adiabatic EGR configurations, respectively.

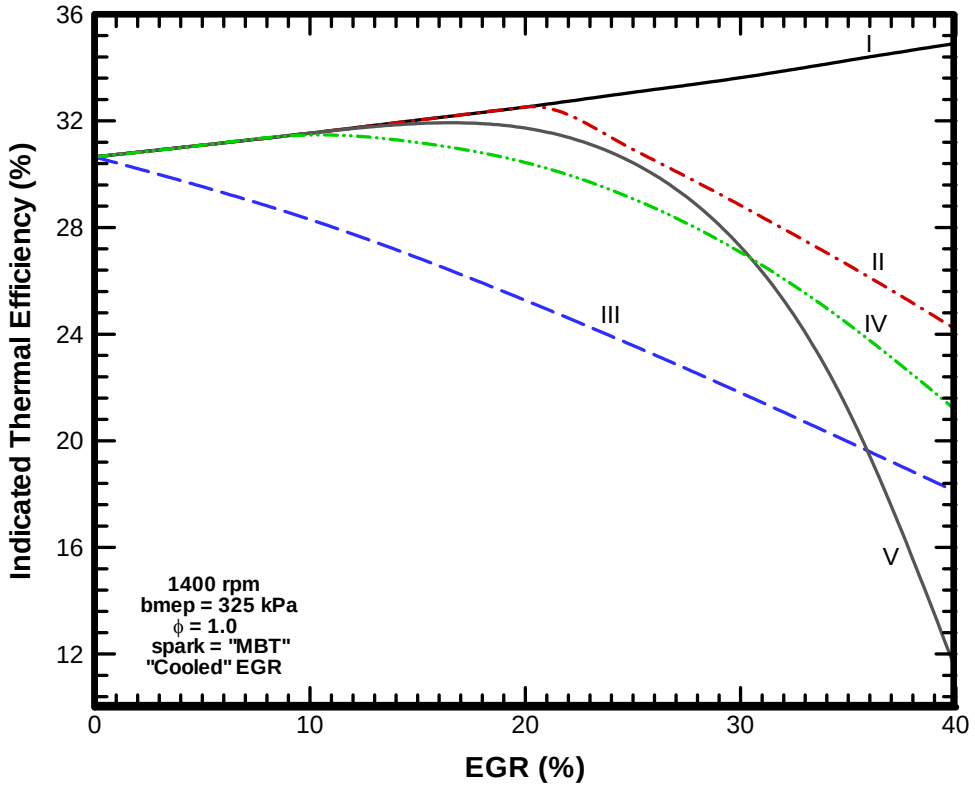

Fig. 33 Indicated thermal efficiency as functions of the percentage of EGR for the five fuel fraction burned schedules for the cooled EGR configuration

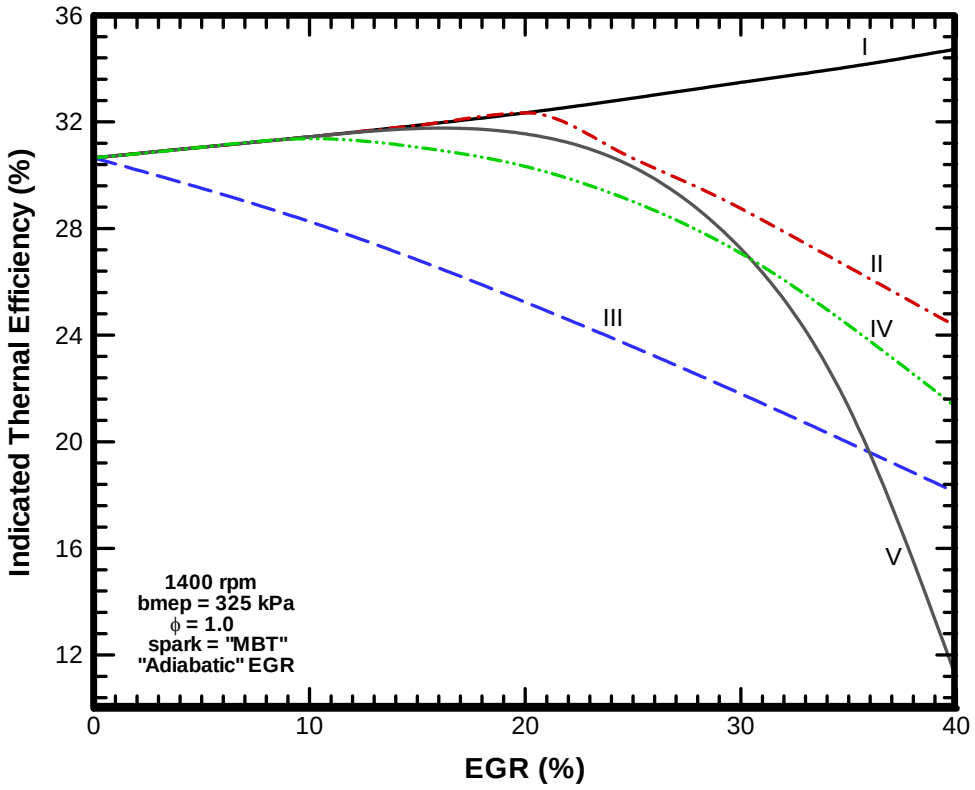

Fig. 34 Indicated thermal efficiency as functions of the percentage of EGR for the five fuel fraction burned schedules for the adiabatic EGR configuration

VITA

Name: Rajeshkumar Shyani

Address: Texas A&M University, Department of Mechanical Engineering,
3123 TAMU, College Station, TX 77843-3123.

Education: Master of Science, Mechanical Engineering, August 2008
Texas A&M University, College Station, TX.

Bachelor of Engineering, Mechanical Engineering, June 2006
G H Patel College of Engineering & Technology,
Sardar Patel University, Gujarat, India.